AD-A086 856   UNITED TECHNOLOGIES RESEARCH CENTER EAST HARTFORD CONN   F/G 20/5
              SHORT PULSE UV-VISIBLE WAVEGUIDE LASER.(U)
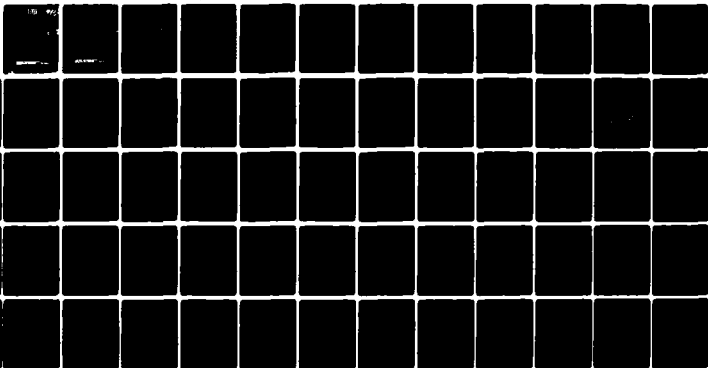   JUL 80   L A NEWMAN   N00014-79-C-0309
UNCLASSIFIED UTRC-R80-924636-1   NL

1 OF 1
AD A
A086856

END
DATE
FILMED
8-80
DTIC

R80-924636-1

LEVEL

SHORT PULSE UV-VISIBLE WAVEGUIDE LASERS

LEON A. NEWMAN

TECHNICAL REPORT
JULY 1, 1980

SPONSORED BY THE OFFICE OF
NAVAL RESEARCH UNDER CONTRACT
N00014-79-C-0309

UNITED TECHNOLOGIES RESEARCH CENTER
EAST HARTFORD, CONNECTICUT 06108

UNITED TECHNOLOGIES
RESEARCH CENTER

UNITED
TECHNOLOGIES.

EAST HARTFORD, CONNECTICUT 06108

R80-924636-1

SHORT PULSE UV-VISIBLE
WAVEGUIDE LASERS

LEON A. NEWMAN

TECHNICAL REPORT
JULY 1, 1980

SPONSORED BY THE OFFICE OF
NAVAL RESEARCH UNDER CONTRACT
N00014-79-C-0309

UNITED TECHNOLOGIES RESEARCH CENTER
EAST HARTFORD, CONNECTICUT 06108

UNITED TECHNOLOGIES
RESEARCH CENTER

UNITED
TECHNOLOGIES

EAST HARTFORD, CONNECTICUT 06108

SECURITY CLASSIFICATION OF THIS PAGE (When Data Entered)

REPORT DOCUMENTATION PAGE	READ INSTRUCTIONS BEFORE COMPLETING FORM

1. REPORT NUMBER R80-924636-1	2. GOVT ACCESSION NO. AD-A086 856	3. RECIPIENT'S CATALOG NUMBER

4. TITLE (and Subtitle) Short Pulse UV-Visible Waveguide Laser,	5. TYPE OF REPORT & PERIOD COVERED Final Technical Report May 15, 1979-May 14, 1980
	6. PERFORMING ORG. REPORT NUMBER R80-924636-1

7. AUTHOR(s) Leon A. Newman	8. CONTRACT OR GRANT NUMBER(s) N00014-79-C-0309

9. PERFORMING ORGANIZATION NAME AND ADDRESS United Technologies Research Center, Silver Lane East Hartford, CT 06108	10. PROGRAM ELEMENT, PROJECT, TASK AREA & WORK UNIT NUMBERS 72

11. CONTROLLING OFFICE NAME AND ADDRESS Office of Naval Research Physics Program, Physical Science Division 800 North Quincy Street, Arlington, VA 22217	12. REPORT DATE Jul 80
	13. NUMBER OF PAGES 62

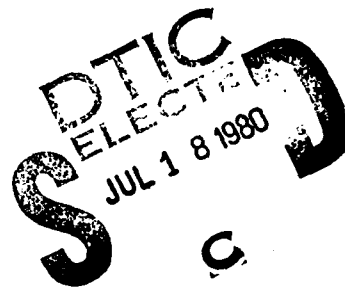| 14. MONITORING AGENCY NAME & ADDRESS(if different from Controlling Office)	15. SECURITY CLASS. (of this report) Unclassified
	15a. DECLASSIFICATION/DOWNGRADING SCHEDULE

16. DISTRIBUTION STATEMENT (of this Report)

Approved for public release; distribution unlimited. Reproduction in whole or in part is permitted for any purpose of the United States Government.

17. DISTRIBUTION STATEMENT (of the abstract entered in Block 20, if different from Report)

Final Technical Report, 15 May 79 - 14 May 80

18. SUPPLEMENTARY NOTES

19. KEY WORDS (Continue on reverse side if necessary and identify by block number)

Nitrogen ion laser, waveguide laser, capillary laser, He-N_2 charge transfer laser, plasma processes in He-N_2 lasers, electron collision processes in He-N_2 laser, capacitively coupled discharge waveguide laser

$He_2(+)$ N_2^+ A

20. ABSTRACT (Continue on reverse side if necessary and identify by block number)

The operation of a N_2^+ ion waveguide laser (4278 Å) excited by charge transfer from He_2^+ created in a capacitively coupled self-sustained discharge is described. In addition, the results of an experimental diagnostic program and a computer modeling program, conducted to explain the general operations of the discharge pumped He-N_2^+ system, are presented. The results of this program indicate upper laser level electron quenching and lower level pumping

DD FORM 1473 EDITION OF 1 NOV 65 IS OBSOLETE
1 JAN 73
S/N 0102-014-6601 |

may be seriously limiting the achievable laser efficiency of this system.

During the course of this study, it was found necessary to measure the pressure broadening coefficient of the $N_2^+(B) \rightarrow N_2^+(X)$ emission by He. The value of this coefficient was found to be 3.5 MHz/Torr $\pm$ 0.7 MHz.

Short Pulse uv-Visible Waveguide Lasers

TABLE OF CONTENTS

PREFACE

Under the present ONR contract and funding provided by a Corporate sponsored

program, United Technologies Research Center is conducting an experimental and

theoretical research program to develop a short pulse uv-visible waveguide laser.

This program is centered around a unique waveguide laser excitation configuration

recently discovered at UTRC. The present technical report, which is based upon a

paper submitted for publication in the IEEE Journal of Quantum Electronics, details

the results obtained by exciting the He-N$_2$ visible laser system in this configuration.

THE N_2^+ WAVEGUIDE LASER: EXPERIMENT AND THEORY[*]

Leon A. Newman
United Technologies Research Center
East Hartford, CT 06108

Abstract - The operation of a N_2^+ ion waveguide laser (4278 $\overset{\circ}{A}$) excited by charge transfer from He_2^+ created in a capacitively coupled self-sustained discharge is described. In addition, the results of an experimental diagnostic program and a computer modeling program, conducted to explain the general operations of the discharge pumped $He-N_2$ system, are presented. The results of this program indicate upper laser level electron quenching and lower level pumping may be seriously limiting the achievable laser efficiency of this system.

During the course of this study, it was found necessary to measure the pressure broadening coefficient of the $N_2^+(B) \rightarrow N_2^+(X)$ emission by He. The value of this coefficient was found to be 3.5 MHz/Torr $\pm$ 0.7 MHz.

I. INTRODUCTION

The operation of a molecular nitrogen ion waveguide laser operating at 4278 Å on the $B^2\Sigma_u^+ \rightarrow X^2\Sigma_g^+$ transition is reported. The motivation for this study was to provide a compact, short-pulse, high repetition rate, efficient laser for applications requiring an optical source in the blue/green region of the spectrum. Previous work on the N_2^+ ion laser achieved by exciting high pressure dilute mixtures of N_2 in helium using both high energy electron beams [1]-[5], and transverse discharges [6]-[9] indicated potential in achieving a number of these characteristics.

In the case of electron beam excitation, best laser performance was achieved using 120 Torr of N_2 in 35 atms of He at 253°K. Laser pulse energies of 80 mJ (5J/liter) were obtained at an efficiency of 3 percent based on the energy deposition in the active volume [3]-[5]. Studies revealed the upper laser level to form mainly by charge transfer processes from helium molecular ions to N_2 [4],[10]. Quasi-cw operation on the 4728 Å transition (v' = 0 → v" = 1), indicating rapid lower level removal, was suggested to occur by an electron capture auto-ionization vibrational relaxation process similar to that occurring in the helium molecular ion [4],[11]. Although laser action has also been achieved using transverse discharge excitation at relatively lower pressures (1 atm - 10 atms), laser pulse energies have been limited to 1-4 mJ (0.15J/liter) at efficiencies in the 0.01 - 0.05 percent range, based on energy stored in the capacitors [6]-[9]. Collins, Carroll, and Taylor have reported on an experimental study of a discharge excited N_2^+ laser stabilized by displacement current preionization [9]. Their results indicate the poor laser efficiency characteristic of discharge excitation is the result of a loss of coupling between the discharge load and the driving circuit caused by a rapidly diminishing discharge impedance. On this basis,

it was concluded that discharge excited N_2^+ laser efficiencies were about 1 percent relative to the energy actually deposited in the gas (intrinsic efficiency), a value comparable to that obtained using e-beam excitation.

In the present investigation, discharge excitation of He-N_2 laser mixtures using the capacitively coupled discharge waveguide laser concept reported previously [12] is examined experimentally and theoretically. Due to the longitudinal type geometry and small active volume, the discharge of this excitation scheme is characterized by a reasonably high impedance ($\sim$ 100 ohms) allowing efficient energy deposition. Because this was precisely a deficiency cited for transverse discharge excitation [9], the potential for achieving a device efficiency of 1 percent coupled with the blue/green wavelength stimulated the study of the He-N_2 system.

Section II presents a description of the general operation of the capacitively coupled discharge and results of the laser experiments while Section III describes the diagnostic experiments conducted to help unravel the operation of the discharge pumped He-N_2 system. A comprehensive kinetics model of discharge, plasma and laser processes has been developed as described in Sections IV and V. Therein, it is shown that while the calculated N_2^+(B) formation efficiency is in the 5-10 percent range for the conditions of this study (consistent with a maximum laser efficiency of 1 percent) the potential device laser efficiency is limited to a value of about 0.1 - 0.2 percent due mainly to strong lower level pumping followed by relatively slow vibrational relaxation.[1] A

---

[1] Device efficiency is defined as the potential energy which can be deposited (i.e., energy stored in the capacitor bank before discharge initiation) divided into the laser energy output.

number of lower level pumping processes were found unique to discharge pumping, thus, representing a fundamental difference in discharge excited N_2^+ lasers as compared to their e-beam excited counterpart. Based on these findings, the experimental results of Collins, Carroll, and Taylor were carefully reevaluated using the present model. Computed discharge and laser properties were found to be in good agreement with those of the present work and it is implied their earlier estimate of a 1 percent intrinsic efficiency for the discharge excited N_2^+ laser was a result of an underestimate of energy deposition.

II. LASER EXPERIMENTS

In Fig. 1 is shown the discharge circuit and a drawing of the discharge tube used in this study. The dielectric waveguide is constructed from a 28 cm Pyrex precision bore capillary tube with a 6.2 mm outer diameter. Three bore diameters of 0.5 mm, 1.0 mm and 1.25 mm were investigated. Three ground return electrodes in contact with the gas were epoxied into three small holes along the length of the tube. Between these wires, 5-cm sections of aluminum foil were wrapped around the tube. The capacitance between these metal foils and the center gaseous conductor forms the coupling capacitance shown in the equivalent circuit of Fig. 1. The split discharge configuration, indicated here, was used to reduce the voltage required to produce E/N values necessary to excite the He-N_2 system at high total pressure. The laser mirrors and gas connections are attached to the capillary tube with teflon fixtures and viton O-rings.

The laser is excited by applying to both of the 5-cm electrodes a negative voltage pulse typically between 50 kV and 60 kV with a risetime of 10 nsec. As depicted in Fig. 2, the gas is initially ($t = t_o$) in a nonconductive state. After the application

4

a)

b)
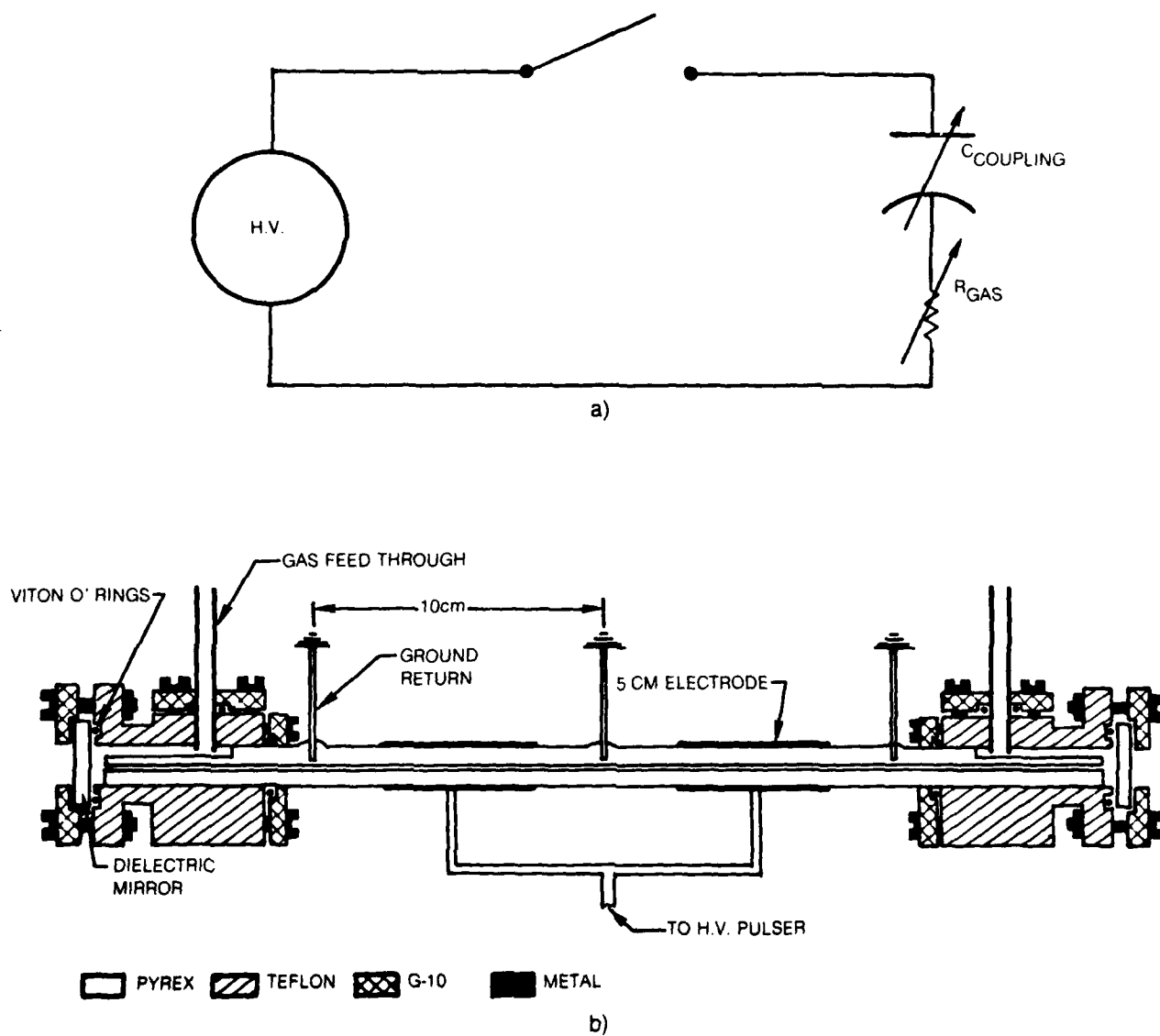
Fig. 1 (a) Equivalent discharge circuit for the capacitively coupled discharge.

(b) Drawing of the discharge tube used in this study.

80—04—120—1

NON-CONDUCTIVE

CONDUCTIVE
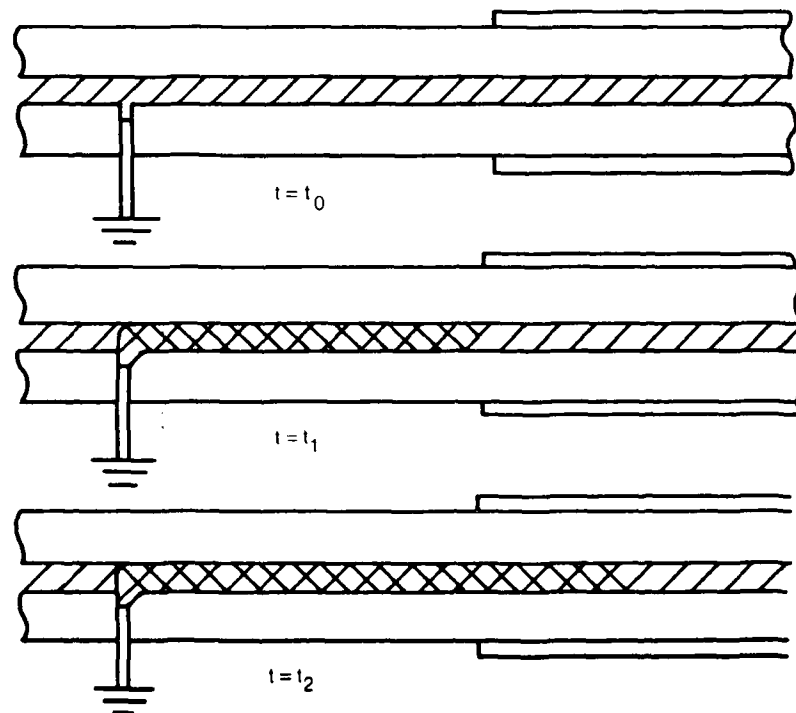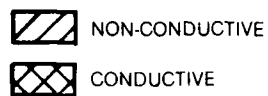

$t = t_0$

$t = t_1$

$t = t_2$

Fig. 2   Sequence of events occurring during the initiation of
the capillary discharge.

6

of the high voltage pulse, the fields developed between the ends of the 5-cm electrodes and the ground wires break down the gas in these regions ($t = t_1$). The initial coupling capacitance is that developed between the ground return wires and the extremities of the 5-cm electrode. The gaseous conductor subsequently formed in these regions allows ground potential to extend within the 5-cm electrodes generating a field across the unexcited gas within the interior of the 5-cm electrodes. This causes breakdown and excitation of the gas within the 5-cm electrodes ($t = t_2$) and increases the coupling capacitance due to a change in conductor geometry. For the case of the 1-mm bore tube, the coupling capacitance was measured to be 13 picofarads when a conductor was substituted for the gas in the bore of the tube. This value of capacitance results in a potential energy deposition per pulse of between 16 mJ and 23 mJ for the applied voltages indicated.

It is to be realized that during the rise of the voltage source, the coupling capacitance charges up through the gas discharge. At this point in time, one-half the energy delivered by the voltage source is stored in the coupling capacitance, the other half being deposited in the gas. In principle, the energy stored in the coupling capacitance can be deposited in the gas by switching the voltage to zero, thus depositing all of the energy supplied by the voltage source. In the present work, only excitation during the rise of the voltage pulse was investigated and no attempt was made to observe operation under the condition of excitation provided by the voltage fall.

Following the design criteria of Abrams [13], a low-diffraction-loss multimode waveguide resonator is formed by placing two flat dielectric mirrors (90 percent and 99 percent reflection at 4278 Å) within a few millimeters of the capillary tube ends.

A perimetric study of the laser operation was conducted in which the gas pressure, gas mixture, applied voltage, gas temperature, and tube bore size were varied. When the gas pressure was varied between 1 and 5 atmospheres, the laser reached threshold at 2 atmospheres and had a very broad optimum at 3.5 atm total pressure for all bore sizes. Likewise, the laser output was found to be relatively insensitive to gas mixture, optimizing at a He:N_2 ratio of 99.85:0.15 when the nitrogen percentage was varied from 0.05 percent to 0.3 percent. Comparable laser amplitude was achieved for the three bore sizes with the best performance obtained with the 1-mm bore tube.

A rather surprising result was the dependence of the laser output on the applied voltage. It was found for applied voltages below 50 kV and above 60 kV, the laser output was sharply reduced. In addition, laser output at the optimum excitation voltage of 55 kV was sporatic with large pulse-to-pulse fluctuations, and optimum laser action was correlated with those particular voltage pulses which yielded lower amplitude, longer duration current pulses. Reduction of laser output at lower voltages can be understood due to reduced pumping at lower electron temperatures. Reduction of laser output at high voltages, however, is not as easily understood and is inconsistent with the results obtained with transverse discharge excitation [8],[9]. With the aid of the kinetic modeling, an explanation for this observation based on the effects of electron-ion recombination is suggested and discussed in more detail later.

The initial gas temperature was reduced to approximately 240°K by blowing cool nitrogen into a jacket surrounding the 1-mm bore tube. The gas pressure was maintained at 3.5 atm, thus the density increased approximately 25 percent. The laser output increased by a factor of three and the side fluorescence at the laser wavelength increased by 25 percent relative to the optimum room temperature results. These results

are consistent with the inverse temperature dependence of the laser output noted previously for e-beam excitation [5].

The best laser performance for room temperature and cooled conditions yielded pulse energies of 1 μJ and 3 μJ, respectively, with a detection limited pulsewidth of 4 nsec. This is well below the 200 μJ expected to occur for 1 percent conversion efficiency. To some degree, this discrepancy can be accounted for by the slow build-up in laser oscillation. In Fig. 3 is shown an accurately timed overlay of the side fluorescence at the laser wavelength and the laser signal. Note that the start of laser oscillation does not occur until the maximum of the fluorescence signal is reached while the peak of laser oscillation occurs when the fluorescence is rapidly decreasing. In addition, no detectable change in the amplitude and temporal shape of the side fluorescence signal was noted under lasing and nonlasing conditions indicating weak saturation of the laser transition. Similar problems in obtaining a high optical extraction efficiency under self-oscillating conditions were noted previously by Collins, et al., with transverse discharge excitation [14]. Thus, it is concluded that laser performance in this device is strongly limited by the cavity build-up time and the short duration of the gain pulse. It is, therefore, not a good measure of the potential extractable energy of the capillary discharge excitation scheme.

III. DIAGNOSTIC EXPERIMENTS

To aid in the determination of the kinetic operation of this device, and therefore its potential with regards to extractable laser energy, a set of diagnostic experiments were conducted on the 1-mm bore tube. A standard set of experimental parameters was established to facilitate the comparison with the computer modeling and the transverse discharge studies of Collins, et al. [9], and are given by a gas temperature,
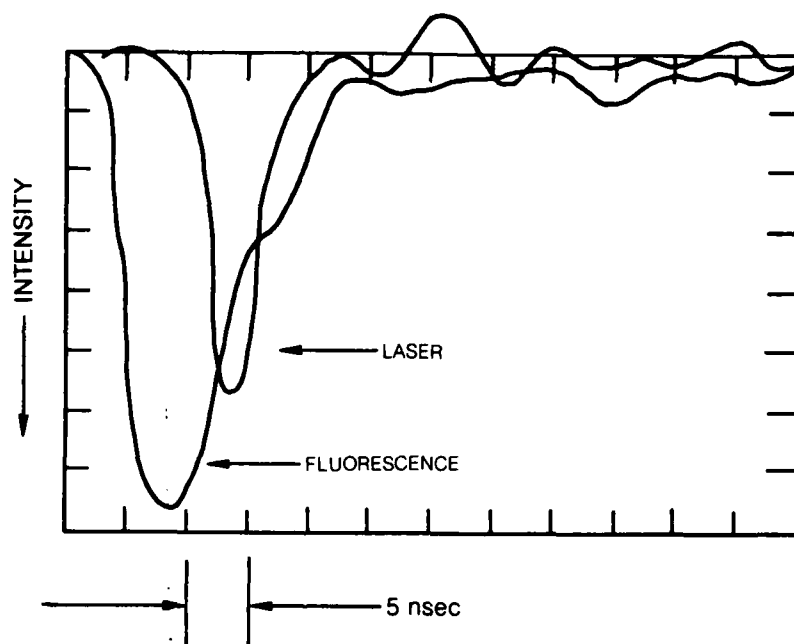
9

Fig. 3 Accurately timed oscilloscope traces of the side fluorescence
at the laser wavelength and the laser signal showing the delay
in laser on-set.

gas pressure, gas mix and applied voltage of 300°K, 3.5 atm, $He:N_2$ - 99.8:0.15 and 50 kV - 80 kV, respectively. The diagnostic experiments included measurements of: (1) the V-I characteristics; (2) the absolute side fluorescence power emitted from the $N_2^+(B)v = 0 \rightarrow N_2^+(X)v = 1$ transition; (3) the relative side fluorescence at 4278 Å versus position along the tube's length; (4) the pressure broadening coefficient of the $N_2^+(B) \rightarrow N_2^+(X)$ transition by helium; (5) the small signal gain-absorption at 3914 Å and 4278 Å; (6) the saturation intensity at 4278 Å; and (7) the electron density via inverse bremsstrahlung absorption of 10.6 μm laser radiation. The details of these experiments are given below.

A. V-I Charactersitics

A high voltage probe (Tektronix P6015) and a 10 Ω resistor in series with the ground return wires were used to monitor the voltage applied to the tube and the discharge current, respectively. Figure 4 presents the output of these monitors for a 55 kV pulser charge voltage under open circuit (b) and normal discharge conditions (a). The open circuit condition, accomplished by filling the tube with three atmospheres of nitrogen, shows the pick-up level in the current monitor due to a small amount of capacitive coupling between the 5 cm electrodes and the ground wires. This pick-up is super-imposed onto the actual discharge current pulse. The discharge current starts near the applied voltage maximum reaching a peak value of approximately 100 amperes and then is modulated during its fall due to the ringing of the applied voltage. This value of peak current corresponds to a peak current density of approximately 3000 amp/cm^2. It should be realized that the applied voltage appears across the coupling capacitance and gas resistance, and that the voltage actually dropped across the gas cannot be measured. The current pulse duration and amplitude were found to vary
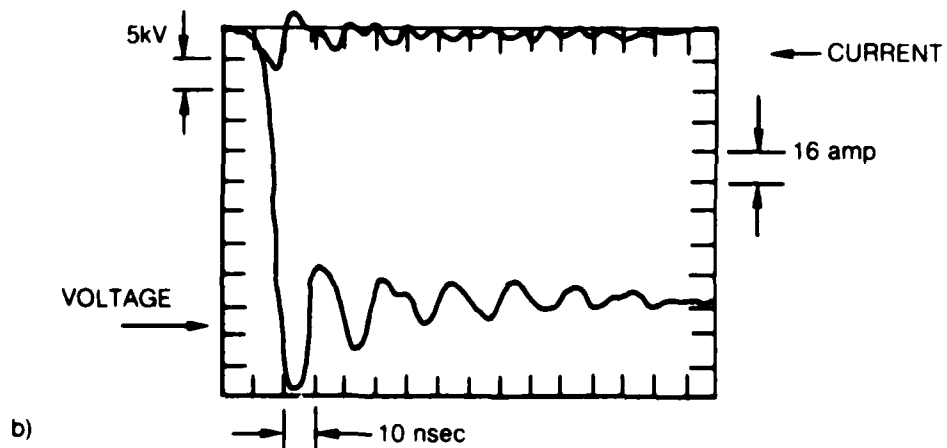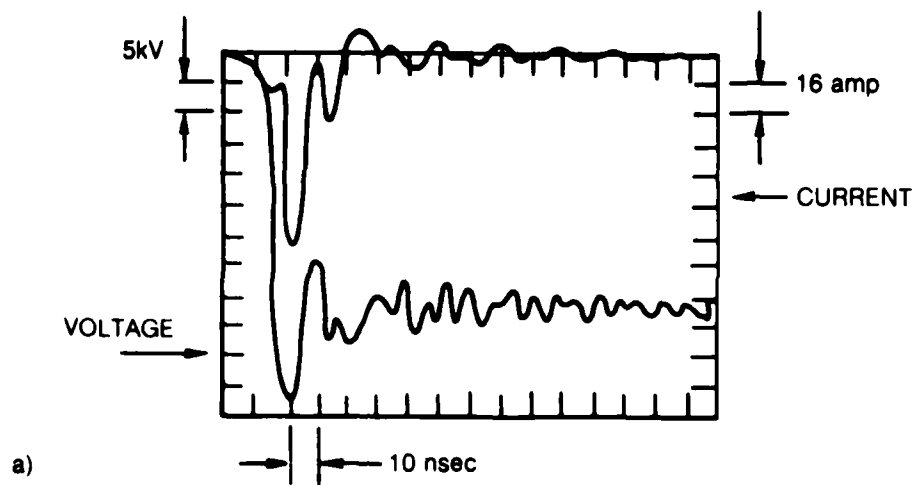
Fig. 4 The voltage and current characteristics for a charge voltage of 55 kV and the standard set of experimental conditions indicated in the text. Normal discharge (a) and open circuit (b) characteristics are shown.

12

considerably from pulse to pulse under lower voltage excitation ($\sim$ 55 kV charge voltage). At higher charge voltages, the current pulse was in the form of a single pulse with a FWHM duration of 5 nsec which increased in magnitude with increasing voltage. As stated previously, optimum laser action was correlated with lower voltage excitation and in particular those voltage pulses which yielded lower amplitude longer duration current pulses.

B. Absolute Side Fluorescence

The filimentary character of the capillary discharge produces a well-defined fluorescence radiation pattern making this excitation geometry particularly well suited for an absolute fluorescent measurement. The absolute value of the fluorescence emitted from the $N_2^+(B)v = 0 \rightarrow N_2^+(X)v = 1$ transition was measured with the experimental configuration shown in Fig. 5. With this arrangement, a precise portion of the total emitted radiation was imaged onto a PMT (1P28) calibrated at 4278 Å with a pulsed dye laser.[2] It was assumed the radiating cylinder emitted into 4π steradians, the active medium was optically thin, and the capillary tube was lossless at 4278 Å; i.e., all the emitted radiation leaves the tube. With these conditions, the PMT signal level was related to the total power emitted from the radiating volume which in turn was related to $N_2^+(B)v = 0$ population with the simple relation

---

[2] The high resolution spectrometer scans conducted for the pressure broadening measurement indicated that the $N_2^+(B)v = 0$ state was the only significant radiator in this wavelength region. The cut-off in the notch filter at short wavelengths eliminated some R branch rotational transitions with high J values from entering the detector; however, this was only a minor fraction of the total spectrum.
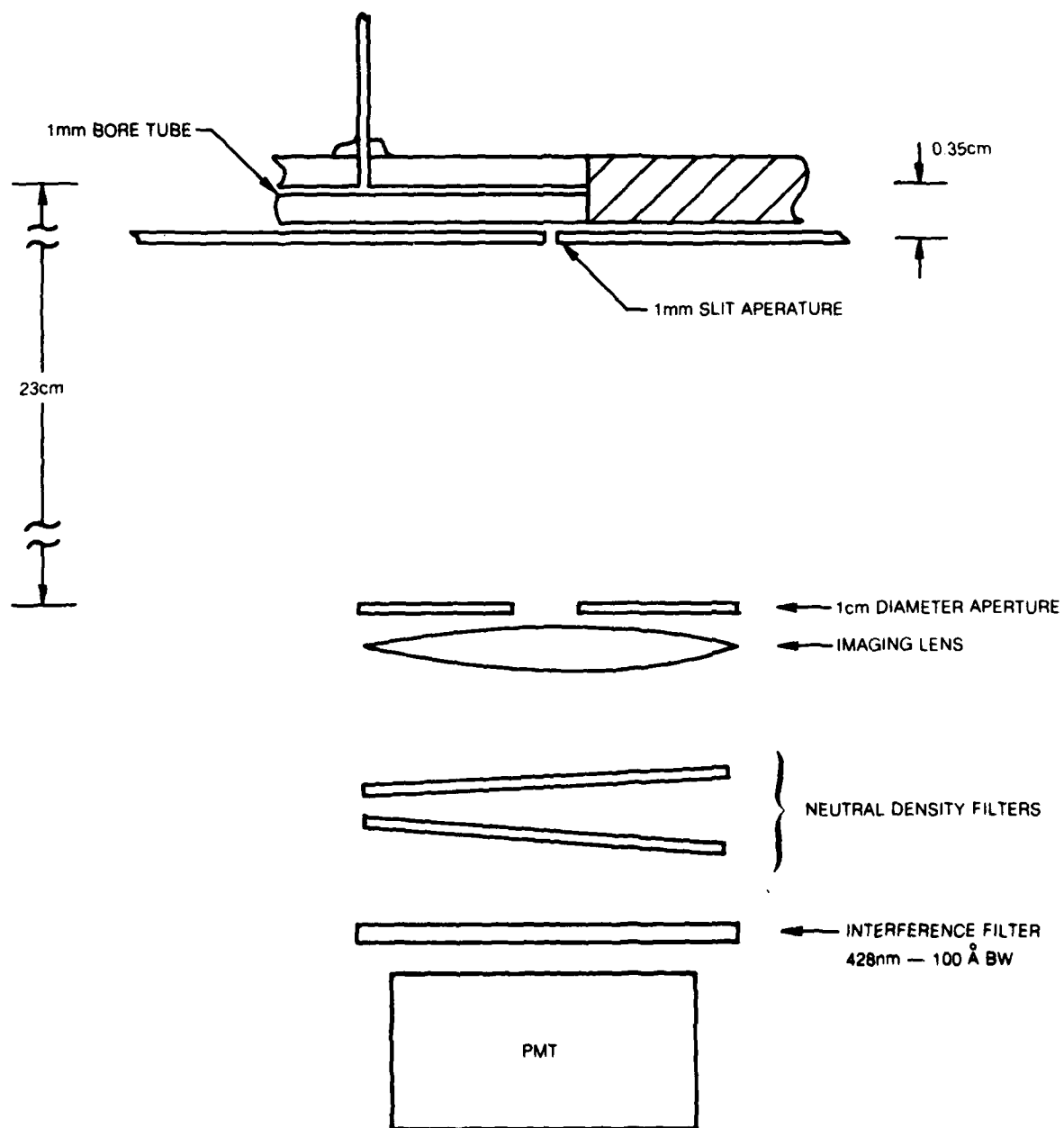
Fig. 5 Experiment configuration used to measure the absolute value of fluorescence emitted by the 4278 Å transition.

14

$$N = \frac{P}{h\nu A} \qquad\qquad (1)$$

where N, $h\nu$, P and A are the population density, photon energy, emitted power density, and transition probability, respectively. The transition probability was taken from the work of Shemansky and Broadfoot [15]. Shown in Fig. 6 are the results of this experiment for a 55 kV charge voltage in which the $N_2^+(B)v = 0$ population is plotted relative to the start of the discharge current pulse.

In order for the population presented in Fig. 6 to be representative of the population along the entire length of the tube, the relative fluorescence versus position along the tube's length must be reasonably constant. A quantitative check of this was made by moving the 1-mm slit aperture along the length of the tube and measuring the relative fluorescence with the notch filter-PMT combination. The fluorescence was observed in 5-cm electrode regions by cutting small windows in the metal foil. As shown in Fig. 7, the relative side fluorescence was found to increase in moving from the ground return electrodes to the extremeties of the 5-cm electrodes and then decrease slightly towards the center of these electrodes. The point at which the absolute measurements were made was found to be a good average of the overall excited state density. The reason for the variation in side fluorescence versus position along the tube is not understood. Such variations were not observed in the rare-gas halide studies [12].

C. Pressure Broadening Coefficient and Stimulated Emission Cross-Section

Accurate stimulated emission and absorption cross sections are necessary to relate gain and absorption measurements to population differences. Reliable cross sections can be calculated if reliable spectroscopic and line broadening data exists. In the case of the $N_2^+(B) \rightarrow N_2^+(X)$ transition, accurate spectroscopic data is available [16], however, the pressure broadening coefficient of this transition by helium has never been measured.
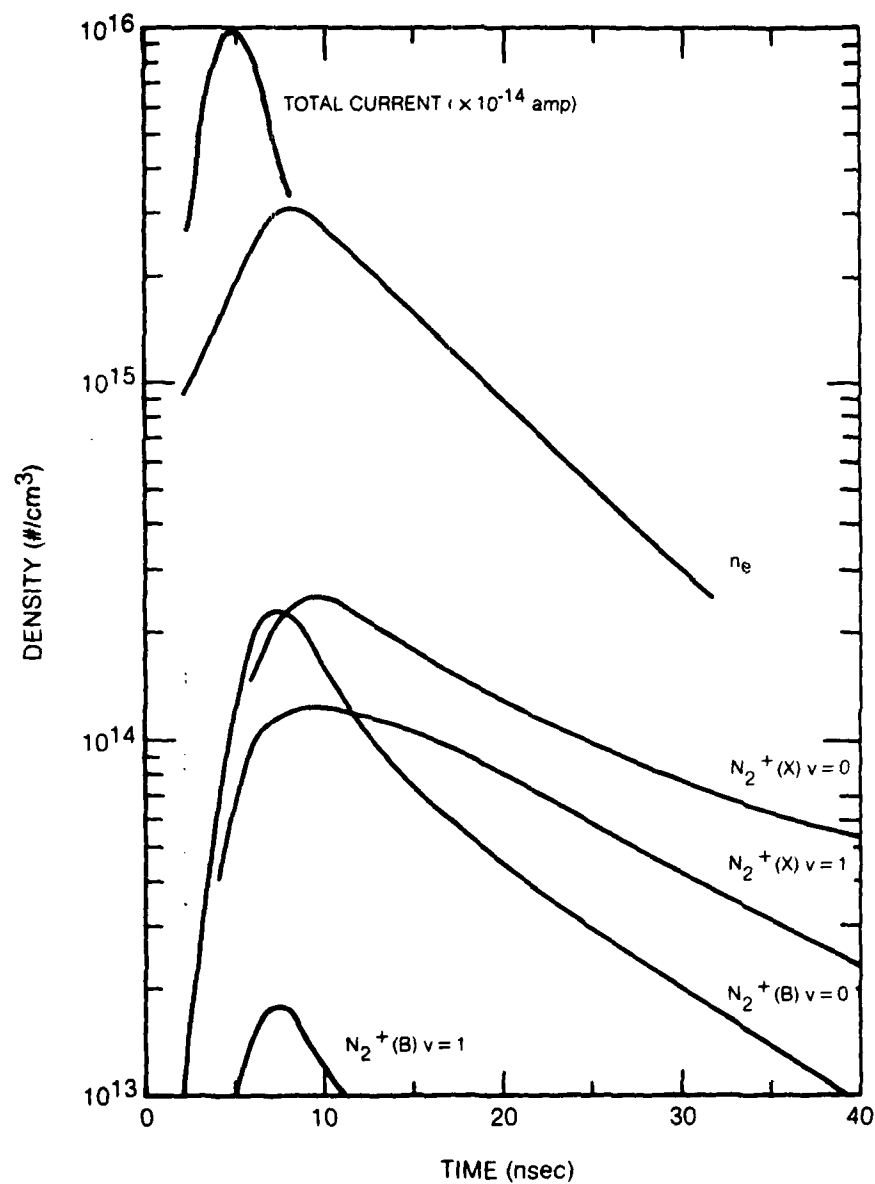
Fig. 6 Temporal evolution of the current, various N_2^+ densities, and the electron density as revealed by the diagnostic experiments.
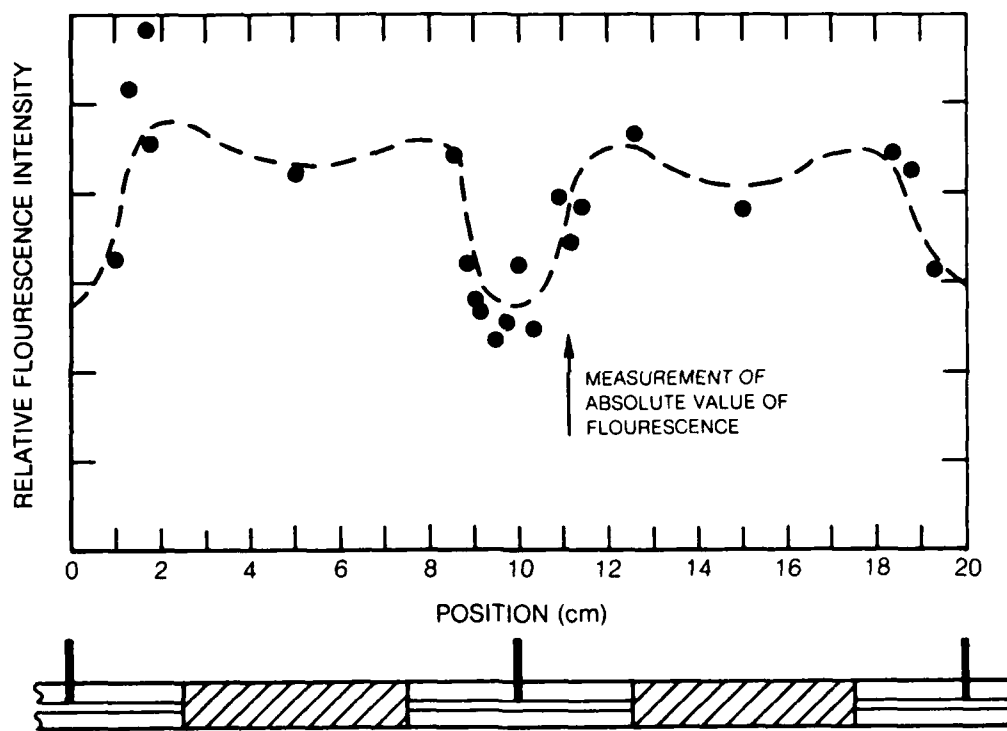
Fig. 7 Relative side fluorescence at 4278 Å vs position along the discharge tube. The solid dots are the measured values while the dashed curves is an artistic average of the measured values.

Because of the need for accurate cross sections, an experiment was performed to estimate this coefficient. The capillary tube, repetitively pulsed at 50 Hz, in conjunction with a 0.5 m spectrometer and a boxcar integrator were used to make high resolution scans of the $N_2^+(B)v = 0 \rightarrow N_2^+(X)v = 0$ rotational emission spectrum versus helium pressure. The experimental emission shapes of a low J value, R branch transition were compared with computed shapes obtained by convolving the spectrometer slit function with Lorenzian profiles of various widths. Comparisons were made at various helium pressures ranging from 5 atm to 13 atm. The effects of gain line narrowing, absorption line broadening, and doublet splitting were found to be unimportant for low J value transitions under weak excitation conditions. The best fit between measured and calculated line shapes resulted in a pressure broadening coefficient of 3.5 MHz/Torr $\pm$ 0.7 MHz.

Using this coefficient, line shape functions for the P-branch bandhead versus helium pressure were determined numerically following the procedure of Peterson [17]. In Fig. 8 is shown the results of this analysis for the $N_2^+(B)v = 0 \rightarrow N_2^+(X)v = 1$ transition. The peak value of the line shape functions in conjunction with the transition probabilities of Shemansky and Broadfoot [15] were then used to calculate the peak stimulated emission cross section versus helium pressure for the blue and UV transitions and are presented in Fig. 9.

D. Probe Laser Experiments

A nitrogen laser pumped dye laser system with a linewidth of 0.2 Å and a 5 nsec FWHM pulsewidth was used to measure gain and absorption on the $v' = 0 \rightarrow v'' = 1$ and the $v' = 0 \rightarrow v'' = 0$ transitions at 4278.1 Å and 3914.4 Å. Due to pressure broadening and bandhead formation, the dye laser linewidth is about the same as the emission
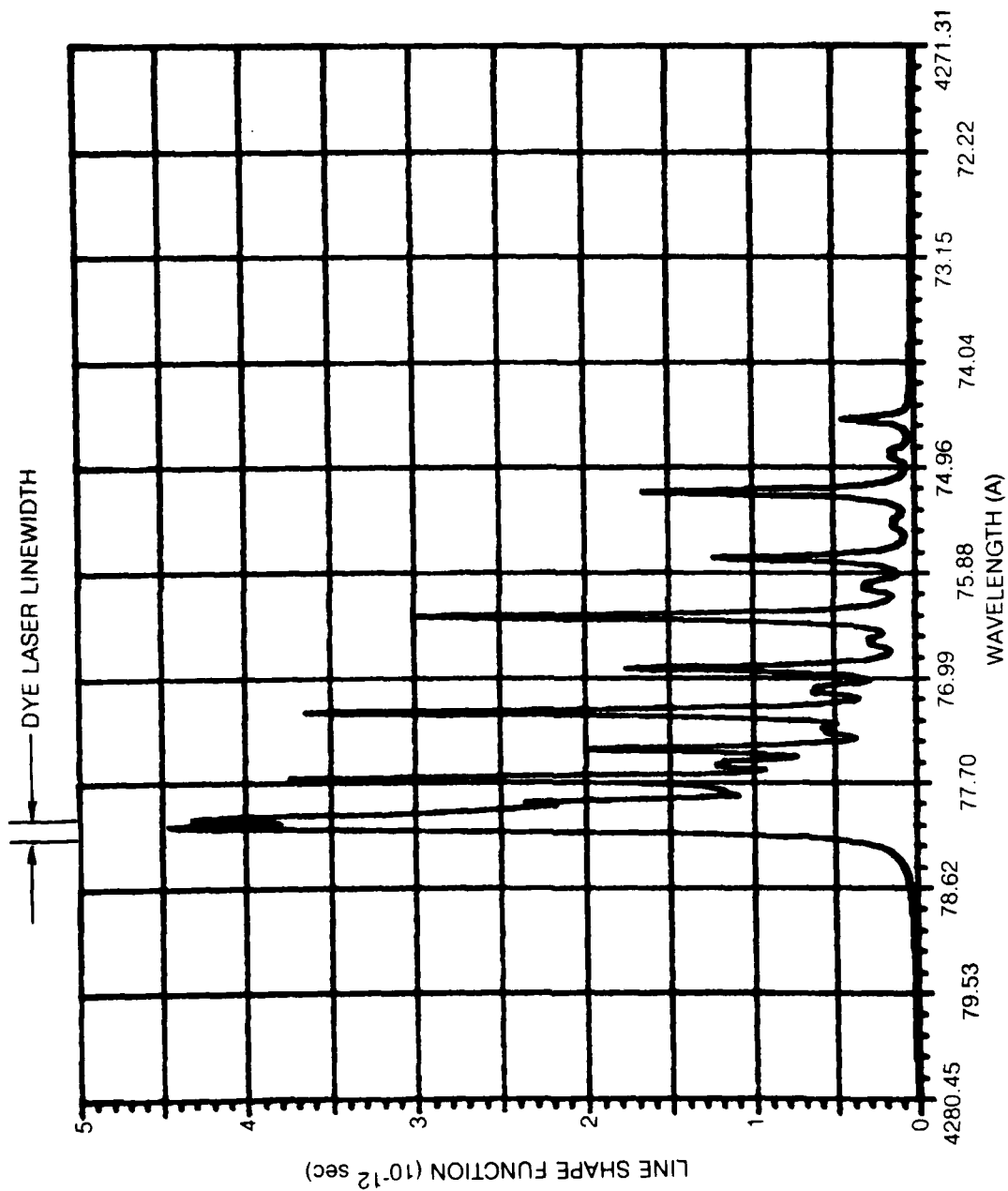
Fig. 8 Calculated lineshape function for the $N_2^+(B)v = 0 \to N_2^+(X)v = 1$ P-branch bandhead at a pressure of 3.5 atmospheres. The relative linewidth of the dye laser used in the diagnostic experiment is indicated.
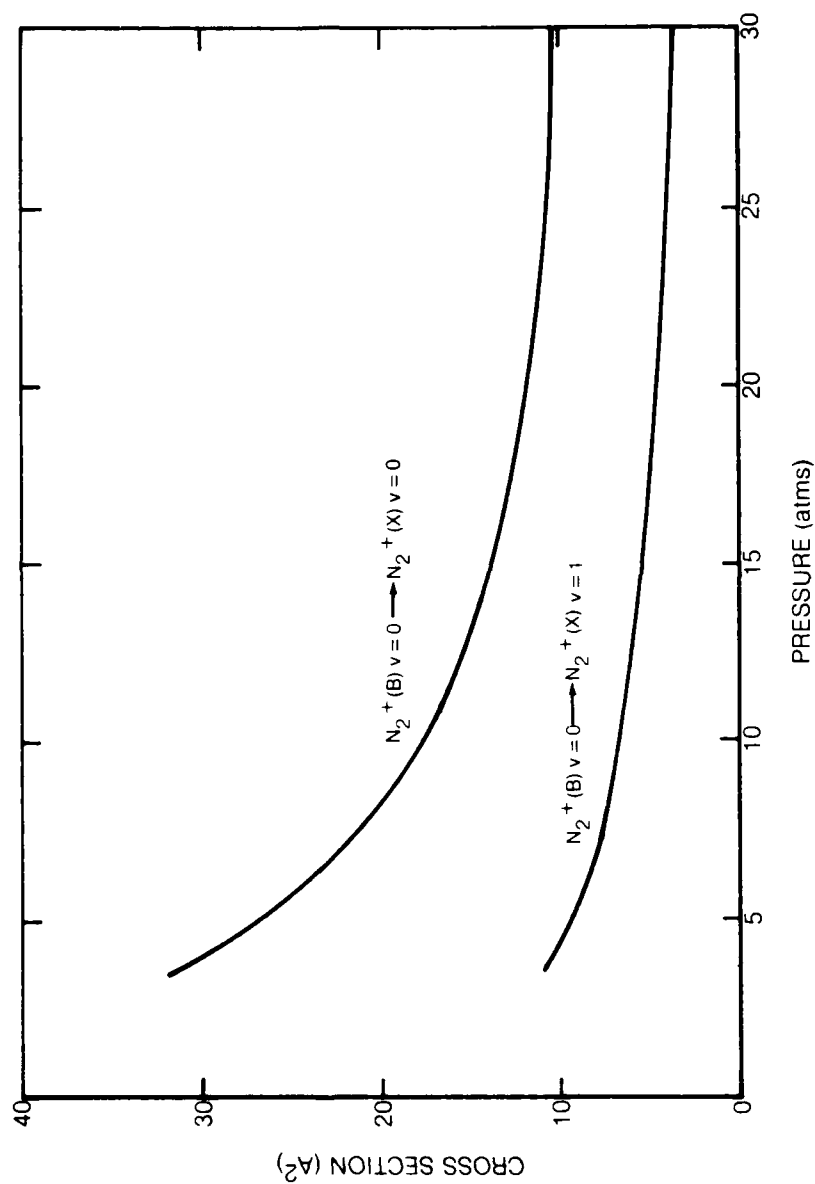
80—04—120—8

19

Fig. 9 Peak value of the stimulated emission cross sections vs helium pressure for the 4278 Å and 3914 Å transitions.

80—04—120—9

20

linewidth at the bandhead peak (see Fig. 8). Because the probe linewidth is not narrow relative to the emission linewidth, the measurements indicated here are expected to slightly underestimate the actual peak gain and absorption.

The arrangement used for this measurement is shown in Fig. 10. A portion of the dye laser beam and bore fluorescence were imaged onto one slit of a 0.5 m spectrometer. By monitoring the magnitude of the bore fluorescence, the spectrometer was adjusted to the bandhead peak for the transition of interest. The dye laser was then adjusted to this wavelength by maximizing the transmission through the spectrometer. The synchronization of the dye laser pulse and the discharge current pulse could be controlled to $\pm$ 2 nsec. Temporally resolved measurements were made by step adjusting the delay of dye laser pulse relative to the discharge current pulse.

Figure 11 presents the ratio of the probe signal output to input relative to the start of the discharge current for both the UV and blue transitions. Also plotted are the associated population differences calculated with the stimulated emission cross sections given in Fig. 9. Because the absorption was very large in the afterglow, only one discharge section was used for the UV transition measurement, resulting in a 10-cm discharge length. In the case of the UV transition, gain occurred during the initial stages of the discharge and then rapidly switched over to absorption at approximately 7 nsec. This result is not surprising given the known self-terminating character of the 3914 $\overset{\circ}{A}$ laser transition. The blue transition also exhibited gain during the initial stages of the discharge as expected. Surprisingly, however, this gain also switched over to absorption at approximately 12 nsec. As seen from Fig. 6, this occurs at a time when the upper level population has dropped to only one-half of its peak value. Using the ΔN values presented in Fig. 11 and the relative value of
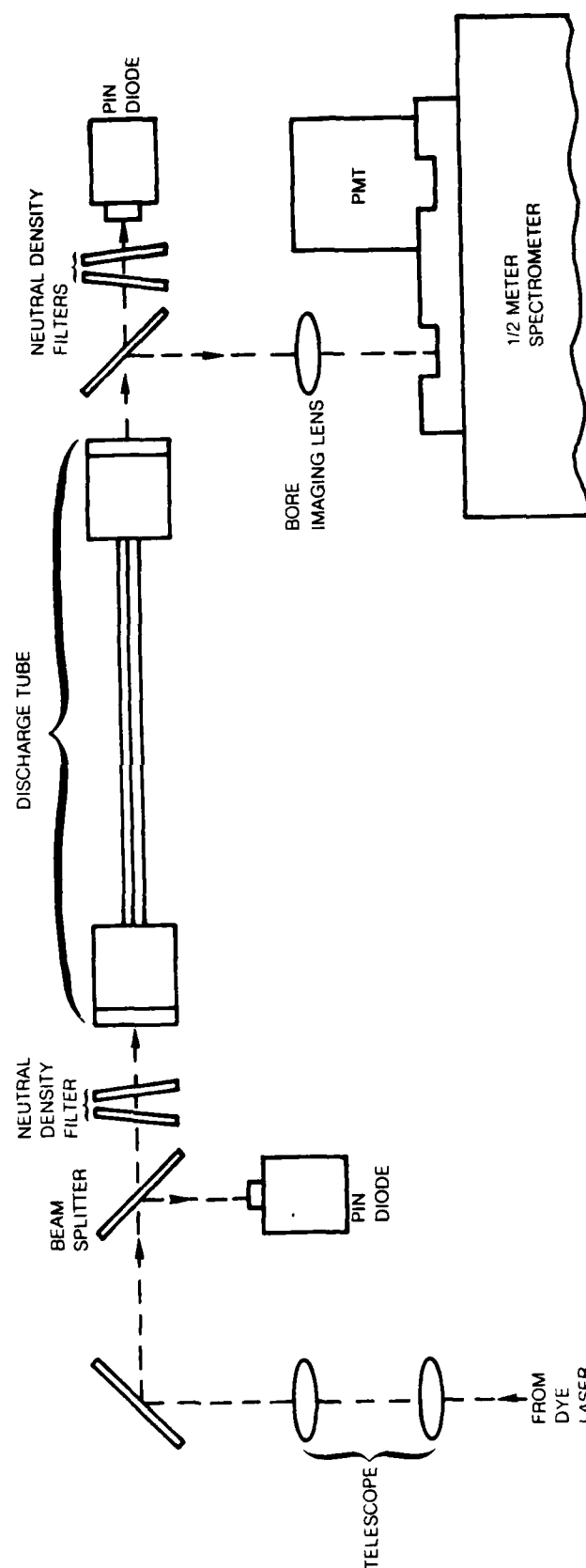
Fig 10. Experimental arrangement used in the dye laser
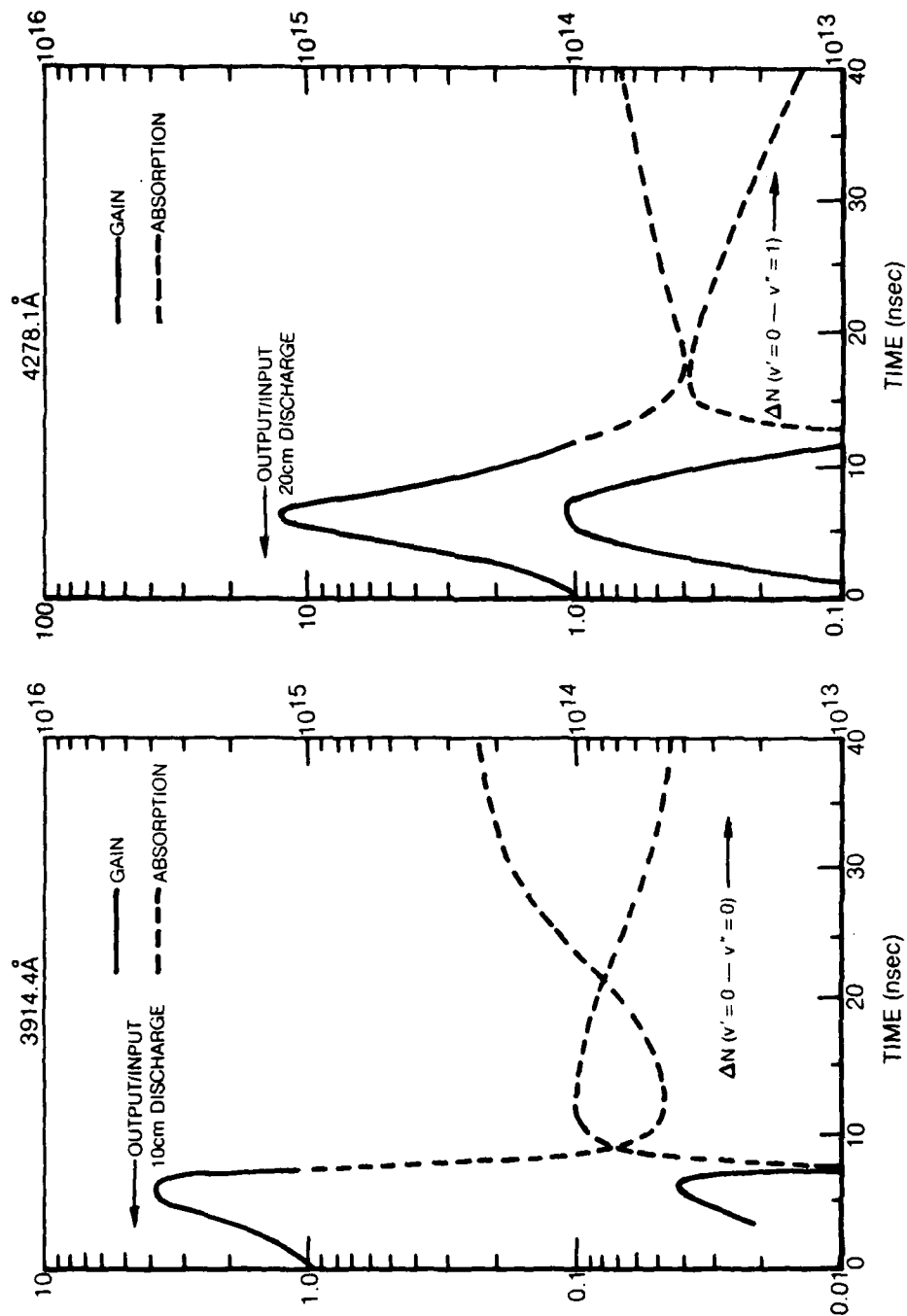gain-absorption measurements.

80-04-120-10

22

Fig. 11 Ratio of the dye laser output to input level referenced to the start of rapid current rise. The ΔN curves were determined with this data and the stimulated emission cross sections given in Fig. 9.

80-04-120-11

fluorescence emitted from the $N_2^+(B)v = 1$ level, the populations of the $N_2^+(X)v = 0$ and 1, and $N_2^+(B)v = 1$ states were related to the absolute value of the $N_2^+(B)v = 0$ population and are shown in Fig. 6. As is clearly evident a lower level population reaching a value greater than one-half the upper level population exists throughout the entire gain pulse for the 4278 Å transition. It was anticipated the $N_2^+(X)v = 1$ level would rapidly relax to the $v = 0$ level through the capture-autoionization process mentioned previously, resulting in an insignificant lower level population. Indeed, the $N_2^+(B)v = 1$ level is apparently rapidly relaxed given its small relative value. That this is not the case for the $N_2^+(X)v = 1$ level implies lower level pumping which can not be compensated by fast-vibrational relaxation is an important process in the discharge pumped He-N_2 laser for the conditions of this study, thus resulting in an extractable laser energy well below the upper level formation energy times the quantum efficiency. It is conceivable that optimum performance of the e-beam excited N_2^+ laser obtained at very high pressure is due in part to an increase in the lower level removal rate through an increase in the V-T vibrational relaxation rate.

When the dye laser was adjusted to the red side of the blue transition bandhead, no obvious absorption was noted to 50 nsec after the discharge, indicating broadband absorption at the laser wavelength is not seriously limiting the optical extraction efficiency.

By placing various combinations of neutral density filters before and after the discharge, the probe laser power density in the capillary tube could be adjusted, providing a plot of output power density versus input power density at 4278 Å. By fitting this curve to the solution of the steady state amplifier equation without a nonsaturable absorber, the saturation intensity was estimated to be between 100 kW/cm^2

and 200 kW/cm^2 [17]. This can be compared to the saturation intensity for transverse discharge excitation of 80 kW/cm^2 obtained by fitting the data of Collins, et al. to the same amplifier equation [14].

An estimate of the potential extractable laser energy at 4278 Å from this device can be made by assuming it is operated as a strongly saturated amplifier. Under this condition, the extracted power is given by

$$P_{ex} = I_s \, \alpha_g \, L \, A \qquad (2)$$

where P_{ex}, I_s, α_g, L and A are the extracted power, saturation intensity, gain coefficient, discharge length, and discharge area. Using measured values of these quantities along with a FWHM gain pulsewidth of 6 nsec, a potential extraction energy of between 12 µJ and 24 µJ is estimated for this device which is still considerably below the 200 µJ, 1 percent conversion efficiency value.

E. Electron Density Measurement

The peak value of electron density is an indicator of the overall degree of ionization, and therefore, an indicator of the amount of discharge energy that ends up producing ions. Because of the discharge configuration, the voltage applied to the gas could not be measured directly, thus precluding an estimate of the electron density from the V-I characteristics. This problem was circumvented by estimating the electron density via inverse bremsstrahlung absorption of 10.6 µm CO_2 laser radiation. This was accomplished by mode matching a 2 W laser beam into the capillary tube with a 25 cm f.l. lens and detecting the transmitted signal with a fast mercury-doped germanium detector. The theory necessary to convert the absorption data into electron density has been dealt with in previous work [19]. For the condition of the present experiment in which the probe laser frequency is much greater than both the plasma frequency

and electron-neutral collision frequency, the electron density and CO_2 laser absorption are related by

$$n_e = 3.73 \times 10^2 \, \nu^2 \, \alpha_a / \bar{\nu}_e \qquad (3)$$

where n_e, ν, α_a and $\bar{\nu}_e$ are the electron density (cm^{-3}), the probe laser frequency (sec^{-1}), the probe laser absorption coefficient (cm^{-1}) and the effective collision frequency (sec^{-1}). Above an E/N value of approximately 4×10^{-17} v-cm^2 ($T_e \sim 2$ eV) the effective collision frequency to neutral density ratio is near constant with a maximum value of 7.9×10^{-8} cm^3/sec [19]. Below this E/N value, the collision frequency gradually decreases. In the present analysis, the maximum value of the collision frequency was used without alteration. Therefore, the electron density inferred from the absorption measurement will represent a lower limit, which is expected to be a good estimate of the actual density during gas break characterized by a high electron temperature (5 eV) but an underestimate during the afterglow characterized by a low electron temperature (0.2 eV).

In Fig. 6 is presented the results of this experiment for the standard conditions. A peak electron density of 3×10^{15} cm^{-3} is inferred. The electron density decay after the peak is not characteristic of a recombination dominated plasma and is most likely a result of the constant collision frequency assumption.

IV. KINETIC MODEL

In the present study, a kinetic modeling program was embarked upon to act as an interpreter and a check of experimental results, to suggest meaningful diagnostic experiments, and to indicate dominant kinetic processes, thereby helping to paint a general kinetic picture of the discharge pumped He-N_2^+ laser, thus revealing its

potential and/or limitations. The precedure used in developing this model is similar to that reported recently by a number of authors in their modeling of various electronic transition lasers [20]-[22]. To follow is a description of the Boltzmann analysis, specific kinetic processes, and the equivalent discharge circuit used to develop this model.

A. Boltzmann Analysis - Excitation Processes

A steady state Boltzmann analysis capable of handling the effects of electron-electron interactions was used to solve for electron impact excitation and ionization rates. A summary describing the general procedure of this calculation has been described recently by Johnson, et al. [21]. The calculation was conducted with a fractional excitation and ionization set at a constant value 10^{-5} and 10^{-6}, respectively.[3]

The inelastic cross section set of the He-N$_2$ system required for the Boltzmann analysis was derived from a number of sources. The nitrogen vibrational excitation cross sections are the same as used in previous work [23]. Nitrogen electronic excitation cross sections from the ground state were taken from the recent work of Cartwright, et al. [24]. Nitrogen ionization, helium metastable excitation and helium ionization were taken from the compilation of Kieffer [25]. Because of the high fractional excitation expected to exist in the capillary discharge, helium metastable ionization and to a lesser degree nitrogen excited state ionization are expected to be important processes. Cross sections for these processes were derived from the

---

[3] The dependence on the distribution function and the resulting excitation and ionization rates on the value of fractional excitation and fractional ionization is expected to have a minor effect on the overall results of the kinetic modeling.

work of Ton-That and Flannery [26], and Long and Geballe [27] for N_2 and He, respectively. In the case of He^* ionization, initial computed results revealed that in order to match up with the measured rate of current rise of both the capillary discharge and transverse discharge, the He^* ionization rate had to be increased by a factor of five above the computed rate using the Long and Geballe cross section which is for ionization from only the lowest lying helium metastable state. This situation is most likely the result of the importance of electron impact ionization of higher lying helium excited states He^{**} and associative ionization of He^{**}. To account for these processes, the Long and Geballe cross section was increased by a factor of five for the Boltzmann analysis.

In Fig. 12 is shown the fractional power transfer curves resulting from the Boltzmann analysis for the standard $He-N_2$ mixture. The power transferred into the seven electronic states and ten vibration states of nitrogen used in the Boltzmann calculation have been lumped into one state symbolized as N_2^* and $N_2(V)$, respectively. Similarly, helium excitation has been lumped into one state He^*. The arrow at the bottom of Fig. 12 indicates typical breakdown E/N values which have been noted for discharge pumping. Therefore, energy will be deposited into the gas at E/N values equal to or less than this value. If the production of the $N_2^+(B)$ upper laser level is to proceed mainly via charge transfer from helium molecular ions; then the pre-curser of these ions, the atomic helium ions, must be produced with a high efficiency to obtain a high laser efficiency. If direct helium ionization were the only process contributing to He^+ formation, the maximum fractional power transferred to He^+ pro-duction of 0.025 (see Fig. 12) coupled with the quantum efficiency would yield a maximum obtainable laser efficiency of 0.3 percent. This value is only marginally
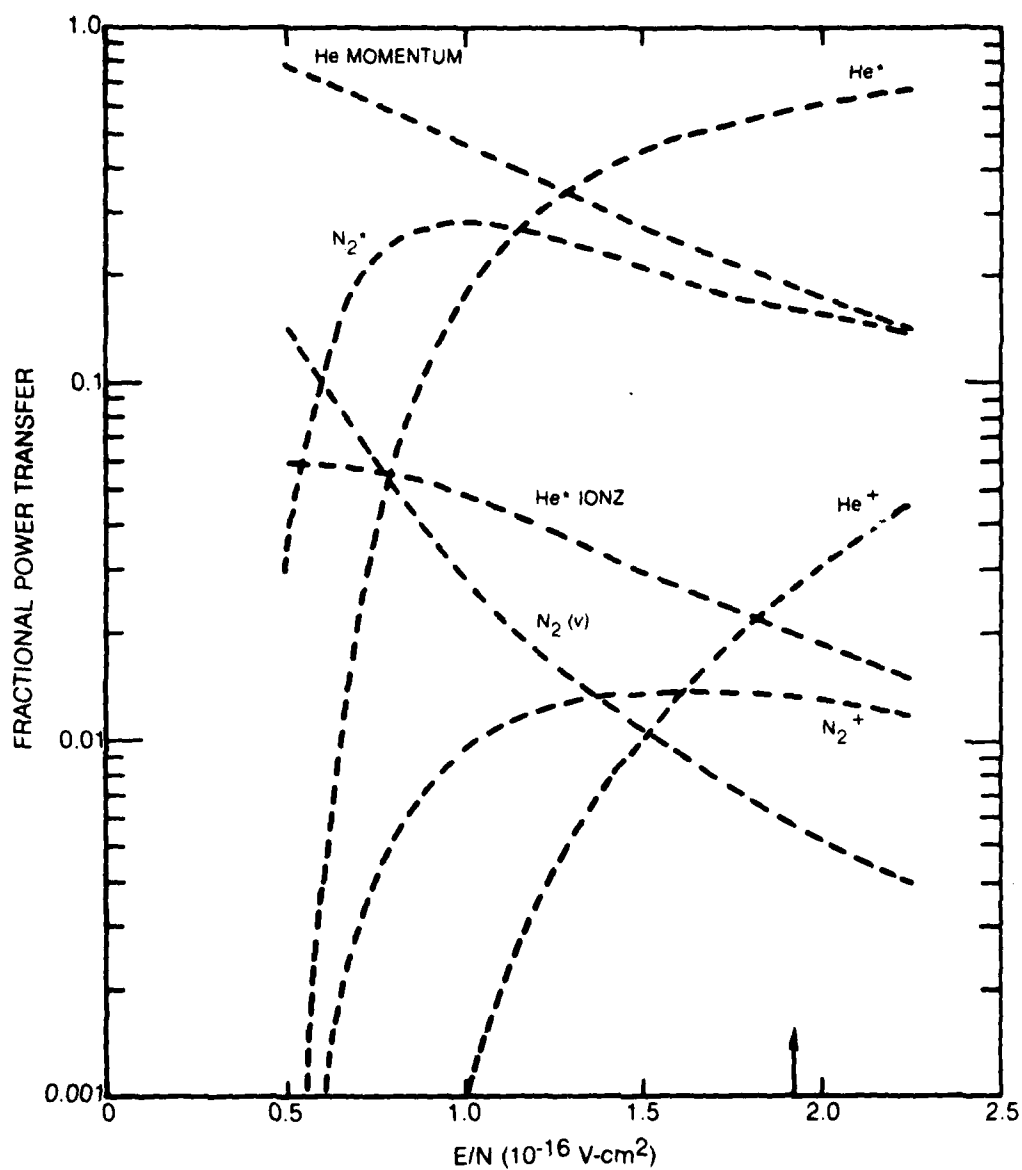
28

Fig. 12 Calculated fractional power transfer curves for a 99.85:0.15 mixture
of He:N$_2$ versus E/N. The arrow at the bottom of the figure indicates
the typical starting E/N value for discharge pumping.

29

sufficient to explain the device efficiencies indicated for transverse discharge amplifier studies [14]. Under the same conditions, however, He^* production occurs with an efficiency of 60 percent. The high current density discharge of present concern results in the creation of a large He^* population thus allowing He^+ production to occur through He^* ionization. As will be shown, multiple step ionization undoubtedly is the dominant route for He^+ production proceeding with an efficiency well above the direct ionization value. Clearly, efficient discharge pumping of $He-N_2$ laser systems through this process will require applied voltages resulting in E/N values above $1.0 \times 10^{-16} \ V-cm^2$.

B. Relaxation Processes

The kinetic sequence used to model the relaxation processes after electron impact excitation is similar to that used by Peterson [17] for modeling the e-beam pumped $He-N_2^+$ laser and to that outlined by Collins, et al. [14]. In Table 1 is listed the dominant processes and associated rate constants used in the present model and the sources from which they were obtained. It is to be noted that diffusion processes will not be important for the experimental conditions and time scale of present interest. There are a number of points which should be noted concerning the reactions listed in Table 1. The branching of the Penning ionization process stated for reaction (1) has been assumed to apply to the three body Penning reaction (2). Penning ionization into the $N_2^+(A)$ state has been lumped in with the $N_2^+(X)$ state. The products produced by the charge transfer reactions (5) and (6) are thought to produce mainly $N_2^+(C)$ and dissociative products with little $N_2^+(B)$ formation [28]. The branching of He_2^+ charge transfer to N_2 is uncertain and is thought mainly to populate the $N_2^+(B)$ state. The branch ratio indicated in reaction 7 and 8 is that suggested by Peterson [17]. The $N_2^+(B)$ quenching processes consisting of dissociative

30

TABLE 1

RELAXATION REACTION RATES USED IN THE He-N_2 MODEL

Reaction	Rate	Reference

Helium Metastable Reactions

1. $He^* + N_2 \xrightarrow{.4} N_2^+(B) + He + e$ 6.9×10^{-11} cm^3/sec   [33], [34]

         $\xrightarrow{.6} N_2^+(X) + He + e$

2. $He^* + N_2 \xrightarrow{.4} N_2^+(B) + 2He + e$ 2.9×10^{-30} cm^6/sec   [33]

         $\xrightarrow{.6} N_2^+(X) + 2He + e$

3. $He^* + He^* \rightarrow He^+ + He + e$ 1.5×10^{-9} cm^3/sec   [30]

4. $He^* + e \rightarrow He + e$ 4.2×10^{-9} cm^3/sec   [30]

Charge Transfer

5. $He^+ + N_2 \rightarrow Products$ 1.5×10^{-9} cm^3/sec   [10]

6. $He^+ + N_2 + He \rightarrow Products$ 2.2×10^{-29} cm^6/sec   [17]

7. $He_2^+ + N_2 \xrightarrow{.75} N_2^+(B) + 2He$ 1.1×10^{-9} cm^3/sec   [35]

         $\xrightarrow{.25} N_2^+(X) + 2He$

8. $He_2^+ + N_2 + He \xrightarrow{.75} N_2^+(B) + 2He$ 1.6×10^{-29} cm^6/sec   [35]

         $\xrightarrow{.25} N_2^+(X) + 2He$

Recombination and Ion Conversion

9. $He_3^+ + e \xrightarrow{.7} He^* + He + e$ (a)   [30]

         $\xrightarrow{.3} others$

10. $He^+ + 2He \rightarrow He_2^+ + He$ 1.0×10^{-31} cm^6/sec   [36]

11. $N_2^+(B) + e \rightarrow N^* + N + e$ (b) cm^3/sec   estimated

12. $N_2^+(B) + N_2 + He \rightarrow N_4^+ + He$ 1.9×10^{-30} (c) cm^6/sec   estimated

TABLE 1 (Cont'd)

Reaction	Rate	Reference
13. $\quad N_2^+(X) + e \rightarrow N^* + N + e$	(b) $\quad cm^3/sec$	[37]
14. $\quad N_2^+(X) + N_2 + He \rightarrow N_4^+ + He$	1.9×10^{-30} (c) cm^6/sec	[36]
15. $\quad N_4^+ + e \rightarrow$ Products	(d) $\quad cm^3/sec$	[37], [38]
16. $\quad N_2^+(B) + e \rightarrow N_2^+(X) + e$	8.0×10^{-8} cm^3/sec	[17]
17. $\quad N_2^+(B) \rightarrow N_2^+(X) + hV$	1.5×10^{7} sec^{-1}	[15]

(a) This reate depends strongly on pressure, electron concentration, and electron temperature (Te). See [30].

(b) 2.68×10^{-6} $Te^{-0.39}$ for $Te > 300°K$.

(c) This process is assumed to saturate above a helium pressure of approximately 2 atmospheres at an equivalent two body rate of 1.0×10^{-9} cm^3/sec.

(d) 5.75×10^{-2} $Te^{-1.8}$ for $Te > 300°K$.

recombination, N_4^+ formation, and superelastic electron quenching (reactions 11, 12 and 16) have never been measured and therefore the values given in Table 1 are estimates. In the case of dissociative recombination, discussions with Michels [29] revealed a large number of favorable dissociative states of neutral nitrogen exist which cross the N_2^+(B) state at its potential minimum. These are precisely the conditions needed for a large dissociative recombination rate, and it was suggested the rate of N_2^+(B) dissociative recombination is at least equal to if not an order of magnitude greater than the rate of N_2^+(X) dissociative recombination. It was also suggested that quenching of the N_2^+(B) state by N_2 should proceed at a rate comparable to or greater than N_2^+(X) quenching by N_2. Therefore, as a first order approximation, the measured dissociative recombination rate and N_2 quenching rate of N_2^+(X) were also used for the N_2^+(B) state. Although by no means certain, the main product channel of N_2^+(B) quenching by N_2 was assumed to be N_4^+ formation. The superelastic quench of the N_2^+(B) state was based on the estimates of Peterson [17]. The recombination rate of He_2^+ with electrons used for reaction (9) corresponds to a collisional-radiative process which depends strongly on pressure, electron density, and electron temperature (see [30]). It was assumed the reaction rate, determined at electron densities and pressure considerably below present values, could be extended to the electron densities and pressures of present concern.

C. Equivalent Circuit

The equivalent circuit shown in Fig. 1 was used to model the flow of energy into the discharge. A problem arises, however, in defining the driving voltage actually appearing across the gas of this simplified model because of the capacitively coupled discharge geometry. This value was approximated in the following manner. The discharge tube was divided into four discharge sections by dividing the two 5-cm

33

electrodes in half. The discharge length associated with one of these sections across which the driving voltage was developed was taken as the distance from the ground return electrode to the center of the bisected foil electrode (3.75 cm). The resulting driving voltage and associated discharge length were then used to define the E/N parameter necessary to solve for the particle densities. The results of the calculation performed on this discharge section were then multiplied by four to obtain the results for the device as a whole.

V. KINETIC MODELING RESULTS

In Fig. 13 is an energy flow diagram for the discharge excited He-N_2 system generally applicable to conditions in which the gas mixture is approximately in the ratio of 0.9985 - 0.0015, He-N_2 and the initially applied voltage generates an E/N value between $1.5 \times 10^{-16} - 2.0 \times 10^{-16}$ V-cm^2. Figure 14 (the counterpart of Fig. 6) presents calculated electron densities, excited state densities, and total currents for the standard conditions and an applied voltage of 55 kV.

A. Energy Deposition

Referring to Fig. 13, it is seen that discharge energy is deposited mainly into He* formation, momentum transfer and N_2^* formation. Ionization then proceeds mainly from a number of secondary processes. For each ionization event that occurs, an electron will of course be produced. Because the peak value of the electron density is a good indicator of the overall degree of ionization and, therefore, an indicator of the amount of discharge energy that ends up producing ionization, it is desirable to have reasonable agreement between the predicted and measured electron density before other comparisons are made. Initial calculations revealed the predicted peak electron density was approximately two times larger than the measured value. The

34

Fig. 13 Energy flow diagram used in modeling the He-N_2 system. This diagram is applicable to high current density, high pressure discharges in which the initial E/N value is in the range of $1.5 \times 10^{-16} - 2.0 \times 10^{-16}$ V-cm^2 and the gas mix is approximately in the proporations of He:N_2 - 99.85:0.15.
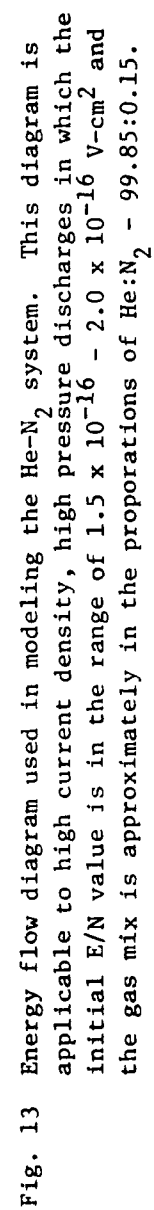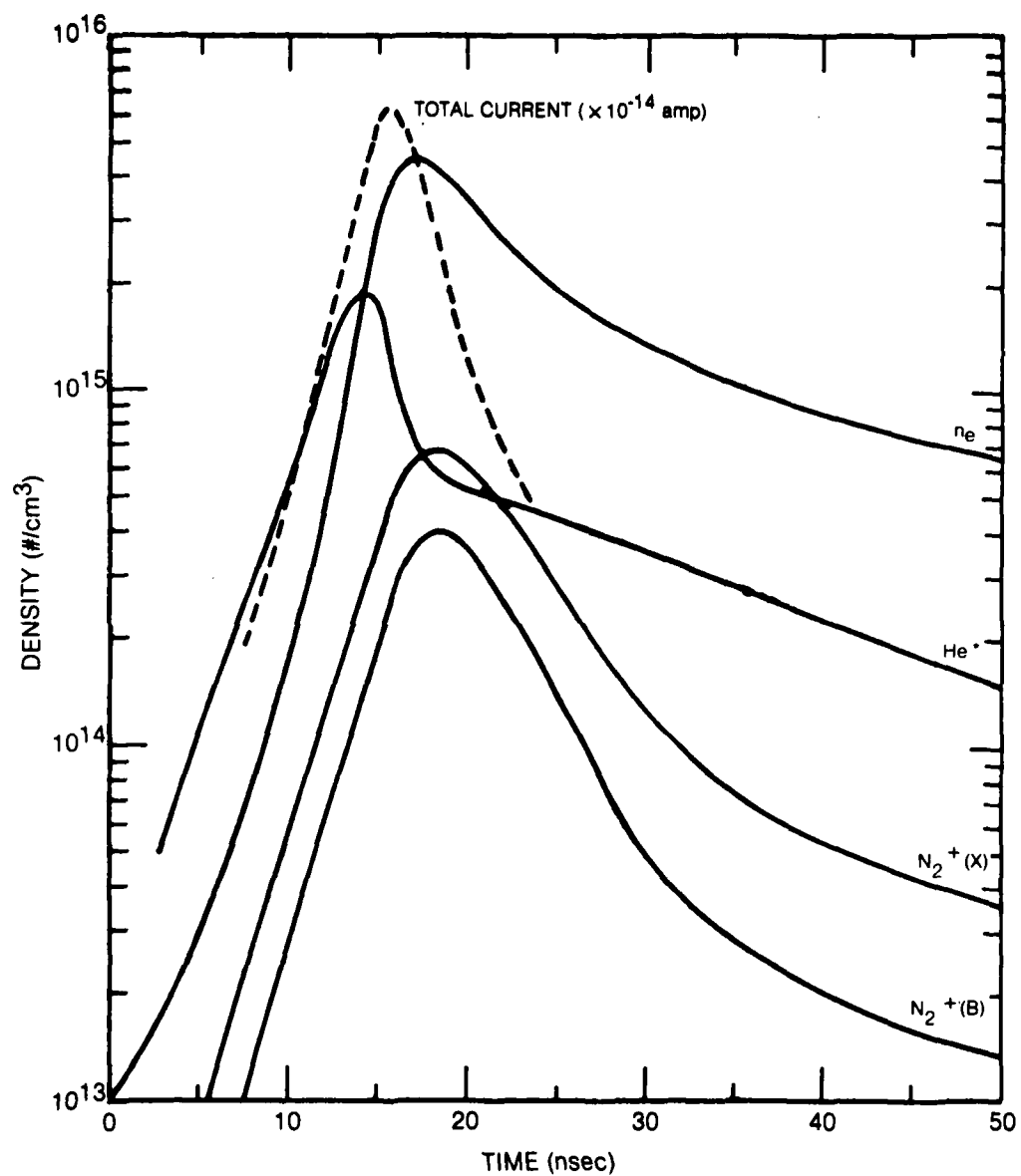
Fig. 14 Temporal evolution of the current, various excited state and ion densities, and the electron density as revealed by the kinetic model.

36

reason for this discrepancy is uncertain. It is thought, however, that this is an indicator that only half of the available energy is deposited at E/N values high enough to produce ionization. This was accounted for theoretically by reducing the coupling capacitance to one-half the experimental value. Therefore, the results presented are for an energy deposition efficiency of 50 percent. Although lower than desired, the reduced amount of energy deposition indicated here cannot in itself explain the less than expected efficiency of the He-N_2 in the capillary discharge configuration.

B. N_2^+(B) Formation

As Fig. 13 indicates, the precurser to charge transfer formation of N_2^+(B) is He^+ formation. A number of processes contribute to He^+ formation but as Fig. 15 shows, He^* ionization is clearly the dominant process contributing over 95 percent of the total during the peak of the current pulse. Because a multi-step ionization process is relied upon for the efficient production of He^+, the discharge pumped He-N_2 system will be intrinsically unstable in its operation, and therefore, will be limited to short pulse excitation. It is interesting to note that during the latter stages of the discharge, the applied E/N drops to values insufficient to produce He*. However, the E/N value is still high enough to ionize the existing He*. This results in the rapid drop in the He* population evident in Fig. 14 during the fall in the current pulse. Thus, excitation provided by the low voltage tail of the excitation pulse can be considered an important contributor to He^+ formation by ionizing the remaining He*. The overall He^+ formation efficiency was calculated to be 14 percent for the standard conditions and an applied voltage of 55 kV.

After the formation of He^+, a branching takes place. For the present condition, approximately one-third of the He^+ charge transfers to N_2 producing products which are
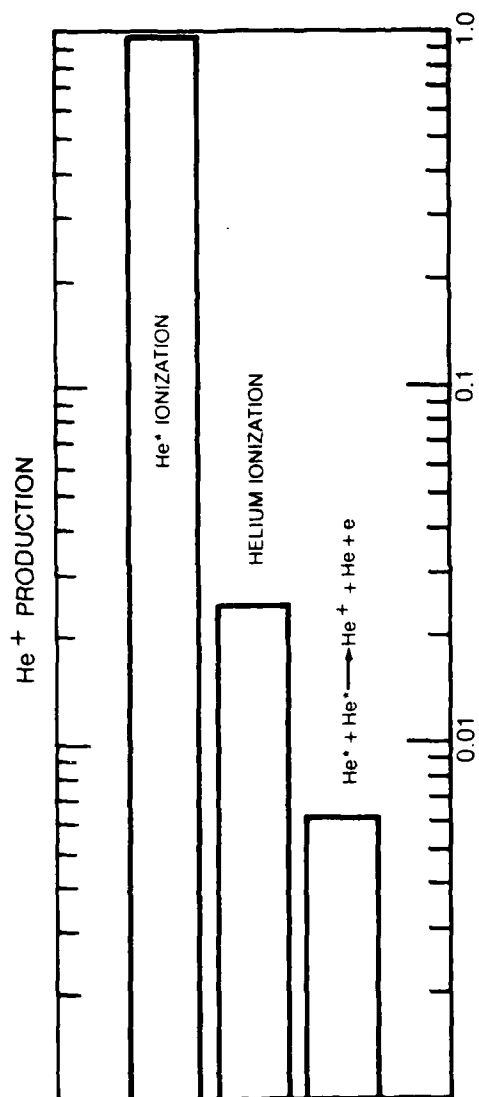
Fig. 15   Fractional contributions to He$^+$ production at the peak of the current pulse.

assumed not to couple to the $N_2^+(B)$ state while the other two-thirds forms He_2^+.

Branching to He_2^+ can be enhanced if the helium pressure is raised due to the square

dependence on helium pressure for ion conversion relative to the linear dependence

on pressure for charge transfer, thus providing a stimulus for higher He pressure

operation.

The He_2^+ formed by ion conversion can then charge transfer to N_2 or recombine

with electrons. Because of the strong dependence of the He_2^+ recombination rate

on the helium density, electron density and electron temperature, the branching ratio

between charge transfer and recombination will also depend on the specific values of

these quantities. The high electron temperature during the current pulse in con-

junction with the inverse electron temperature dependence of the He_2^+ recombination

rate leads to only a 4 percent loss of He_2^+ to recombination as shown in Fig. 16.

After the excitation pulse, the electron temperature will drop to a value deter-

mined by the balance between electron heating due to superelastic collisions and

excited state – excited state ionization and loss due to momentum transfer. In a

recent study by Gand, et al. [31], the electron temperature in the afterglow of a

high current high pressure He discharge was estimated to be 2000°K. Because the

excited state, electron and background densities of the present work are very similar

to those determined by Gand, et al., it is assumed the electron temperature drops to

a value of 0.2 eV (2400°K) in the afterglow with no applied field. Thus, the present

condition of high pressure and high electron density coupled with a 0.2 eV afterglow

electron temperature results in a dramatic increase in the destruction of He_2^+ due to

recombination in the afterglow. As shown in Fig. 16, the contribution of recombina-

tion to He_2^+ quenching increases from 4 percent during the current pulse to 28 percent
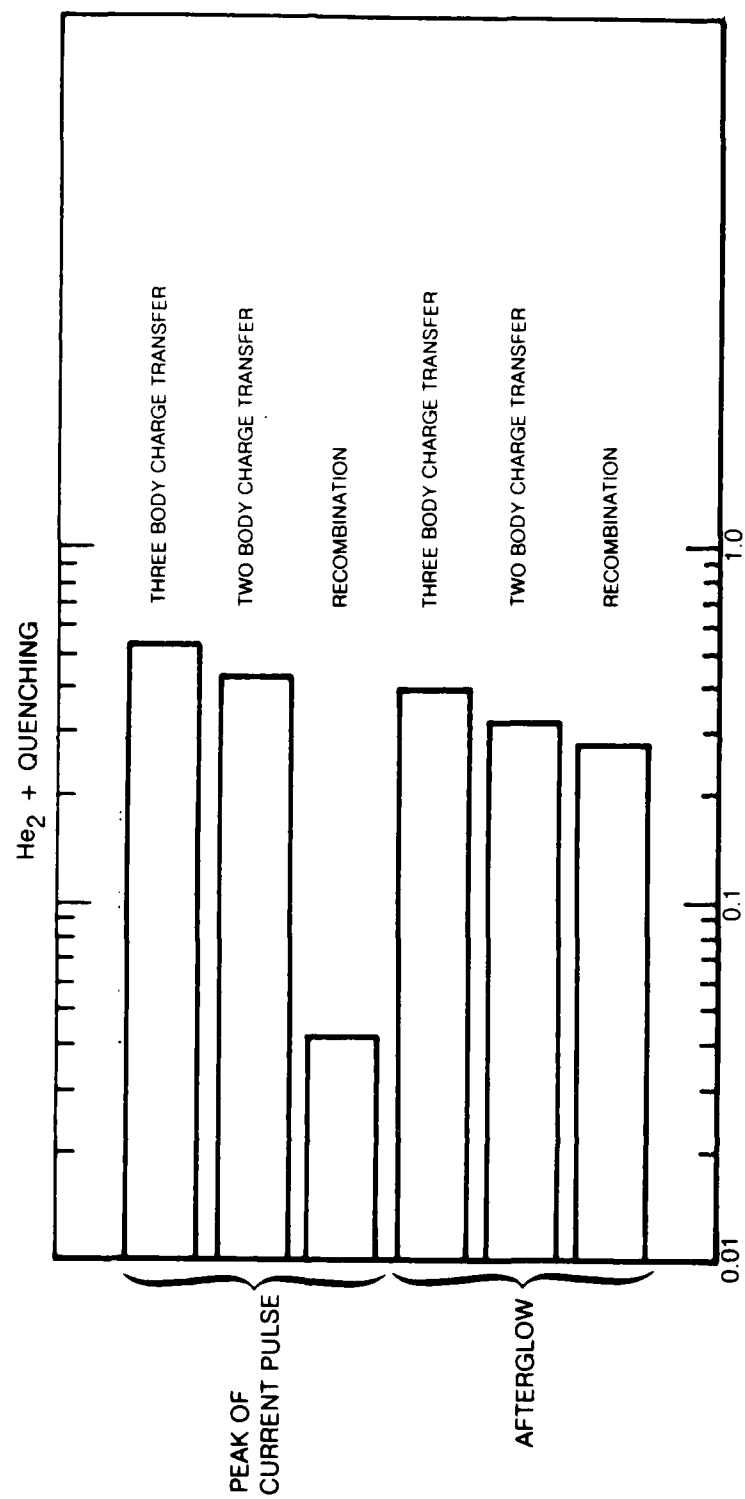
Fig. 16 Fraction contribution to He_2^+ quenching at the peak of the current pulse and during the afterglow.

in the afterglow. For the present conditions in which the applied voltage is 55 kV, the increase in He_2^+ recombination in the afterglow had only a minor effect on the integrated energy flowing through He_2^+ charge transfer branch because most of the He_2^+ quenching occurred during the current pulse when the electron temperature was high. However, when the applied voltage was increased, the resulting calculated current pulse increased in magnitude and decreased in duration. This in turn resulted in a large electron density which very quickly cooled to the assumed 0.2 eV electron temperature. Under these conditions the bulk of the He_2^+ quenching could not occur during the current pulse resulting in well over half of the energy flowing through He_2^+ state going into recombination rather than charge transfer. These results suggest that it is undesirable to excite the $He-N_2$ system with a very short intense current pulse in which the current pulse duration is comparable to the time constant for He_2^+ charge transfer. In this respect, a certain amount of circuit inductance may be desirable for $He-N_2$ discharge excitation because it will limit the magnitude of the current pulse while increasing its temporal duration.

Although there are a number of processes which can contribute to $N_2^+(B)$ formation, the modeling indicates (see Fig. 17) charge transfer to be the dominant process with Penning ionization a distant second. In the afterglow, the He_2^+ population quickly decays. Penning ionization then takes over as the dominant $N_2^+(B)$ formation process resulting in the low level tail of the $N_2^+(B)$ population evident in the 30 nsec - 50 nsec region of Fig. 14. The $N_2^+(B)$ formation efficiency including the 50 percent reduction in energy deposition was calculated to be 7 percent. If 100 percent optical extraction could be achieved, this upper level production efficiency in conjunction with the 15 percent quantum efficiency would yield a laser output of 200 μJ with a device

$N_2^+(B)$ PRODUCTION

TWO BODY CHARGE TRANSFER

THREE BODY CHARGE TRANSFER

TWO BODY PENNING

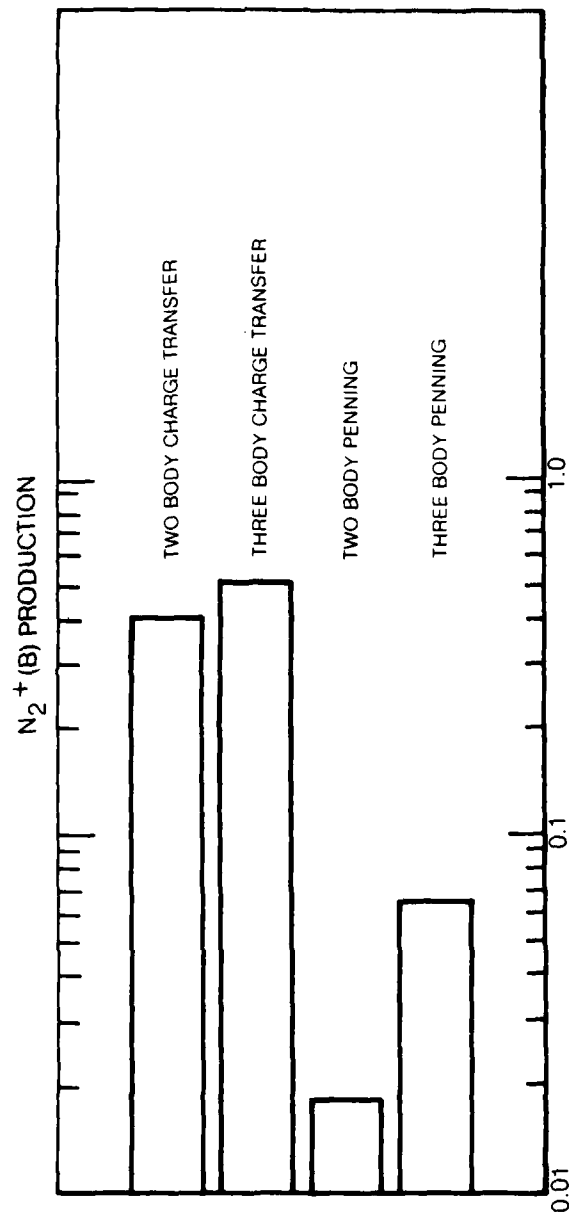THREE BODY PENNING

0.01   0.1   1.0

Fig. 17 Fraction contribution to $N_2^+(B)$ production at the peak of the current pulse.

efficiency of 1 percent. This is clearly well above the 12 - 24 μJ potential extraction energy estimated from the experimental results. These results suggest that upper level production may not be the dominant limiting factor to actual laser performance.

C. $N_2^+(X)$ Formation

In addition to charge transfer and Penning ionization, a number of other processes were found to contribute significantly to $N_2^+(X)$ formation which included superelastic deactivation of $N_2^+(B)$, ground state nitrogen ionization and excited state nitrogen ionization. As Fig. 18 reveals, there is no single process which dominates $N_2^+(X)$ production in contrast to $N_2^+(B)$ production. The summation of these processes results in a calculated $N_2^+(X)$ population which is actually greater than the $N_2^+(B)$ population as shown in Fig. 14. These results clearly indicate that a significant amount of lower level pumping is expected to occur in the discharge pumped He-N_2 system which could account for the large estimated lower level population suggested by the experimental results.

It is of importance to note that a number of these processes, including N_2 ionization, N_2^* ionization and penning ionization, are not expected to be important in direct e-beam excition of the He-N_2 system [17]. As indicated in Fig. 18, elimination of these three processes would decrease the lower level pumping rate by approximately 40 percent and may represent a point of departure in the comparison of discharge and e-beam pumping of the He-N_2 system.

D. $N_2^+(B)$ Quenching

Based on the estimates given previously, quenching of the $N_2^+(B)$ state due to electrons and ion conversion is predicted to be very fast. This result is consistent

N$_2$$^+$(X) PRODUCTION

TWO BODY CHARGE TRANSFER

THREE BODY CHARGE TRANSFER

SUPER ELASTIC QUENCH OF N$_2$$^+$(B)

N$_2$ IONIZATION

N$_2$* IONIZATION

TWO BODY PENNING

THREE BODY PENNING

SUMMATION FIRST THREE
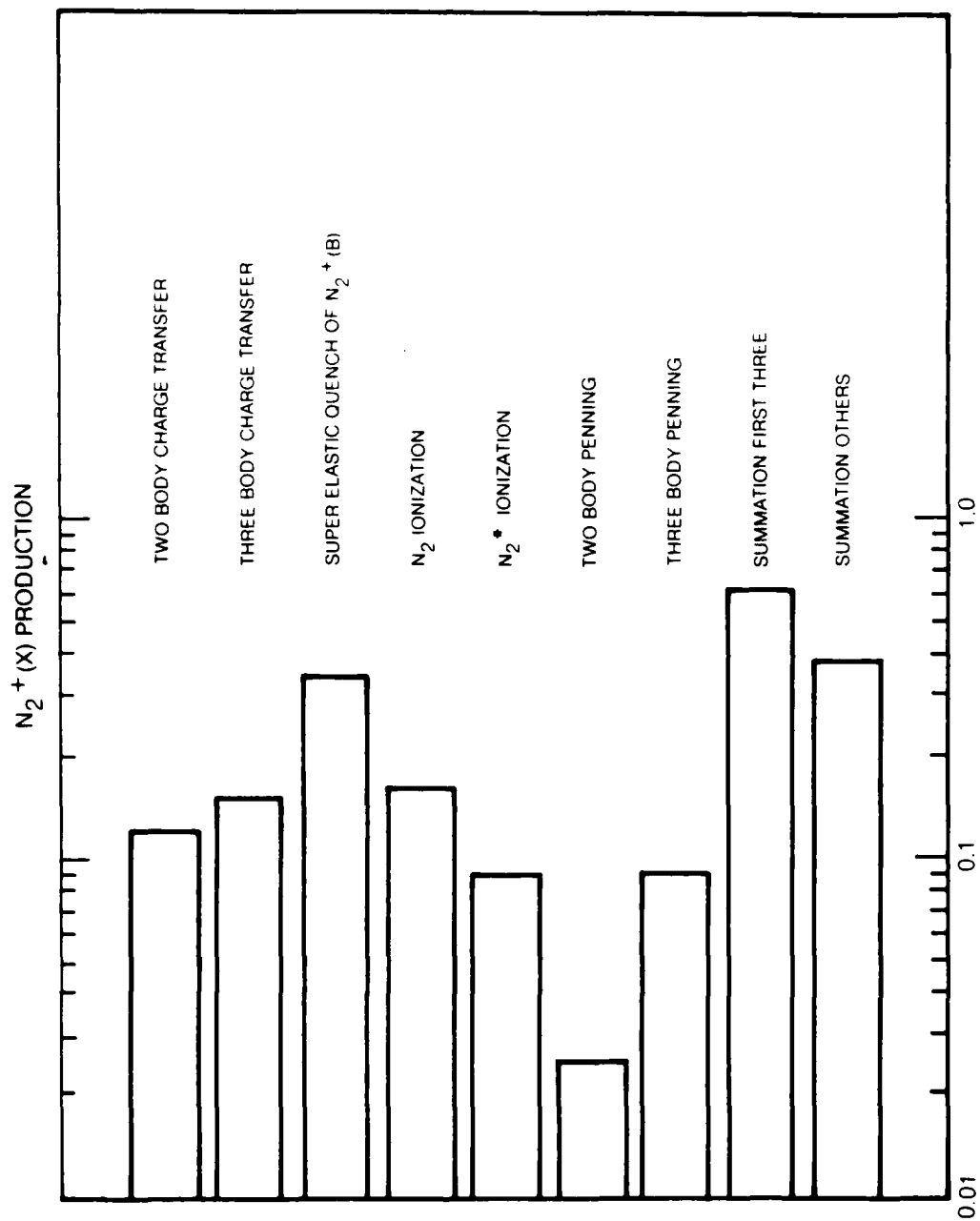
SUMMATION OTHERS

1.0

0.1

0.01

Fig. 18 Fraction contribution to N$_2$$^+$(X) production at the peak of the current pulse.

with the rapid decay in the side fluorescence emitted from $N_2^+(B)$ state at the end of the current pulse. Concentrating on Fig. 19, it is seen that superelastic quenching dominates the $N_2^+(B)$ decay due to the high electron density and the insensitivity of superelastic quenching to the electron temperature. The lifetime of the $N_2^+(B)$ state during the discharge (combining all quenching processes) is calculated to be 1.5 nsec. In the afterglow, the electron density decays and the electron temperature drops to 0.2 eV resulting in an increase in the dissociative recombination rate and a decrease in superelastic quenching. These effects tend to cancel each other resulting in an afterglow $N_2^+(B)$ lifetime of 1.4 nsec. Comparison of the initial decay of the measured and predicted $N_2^+(B)$ state population given in Figs. 6 and 14, respectively, suggest that lifetimes of this magnitude are not unreasonable.

Using the above calculated lifetime, the saturation intensity of $N_2^+(B)v' = 0 \rightarrow v'' = 1$ transition can be estimated assuming no lower level bottlenecking with the relation

$$I_{sat} \approx \frac{h\nu}{\sigma_s \tau_T} \tag{4}$$

where $h\nu$, σ_s and τ_T are the photon energy, stimulated emission cross sections and total upper level lifetime. Using the stimulated emission cross section of 1.1×10^{-15} cm^2 given in Fig. 9, a saturation intensity of 300 kW/cm^2 results. This is somewhat above the experimental estimates of this number of 100 kW/cm^2 – 200 kW/cm^2 given previously. This discrepancy may be a result of a slow lower level removal rate under the present experimental conditions which tends to reduce the saturation intensity.

It is of importance to examine the potential effects of electron quenching on the achievable gain in this system with a steady state analysis. Solution of the steady
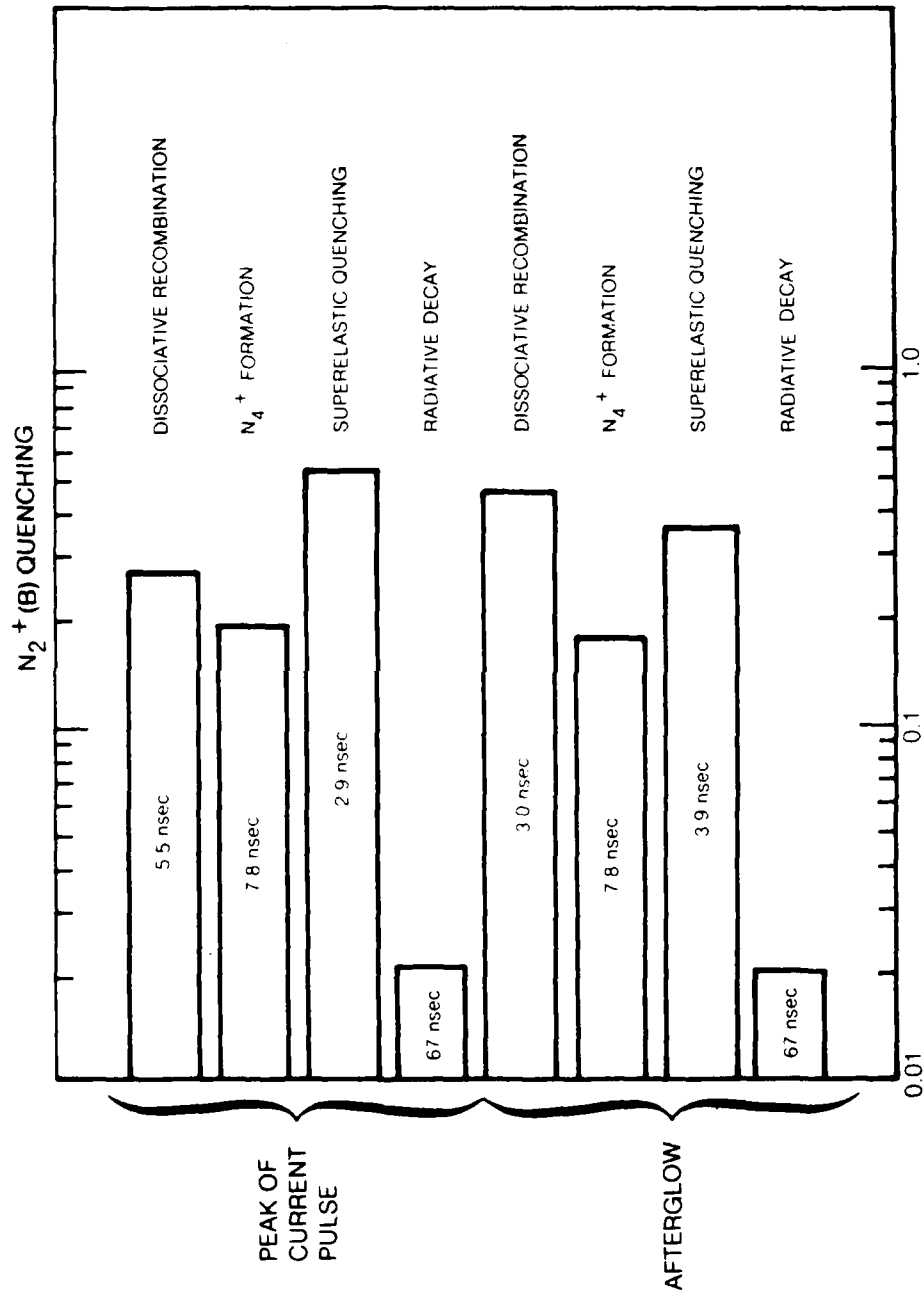
Fig. 19 Fraction contribution to $N_2^+(B)$ quenching at the peak of the current pulse and during the afterglow. Time constants for each process are given in the bar graphs.

state equation for the $N_2^+(B)$ population including only the dominant processes results in the following expression

$$N_2^+(B) = \frac{He_2^+ (N_2 k_7 + N_2 He k_8)}{n_e (k_{11} + k_{16}) + N_2 He k_{12}} \tag{5}$$

where He, N_2, etc., are the population densities of helium, nitrogen, etc., and the k_N values are the rate values given in Table 1 for the Nth number process. The He_2^+ and n_e density indicated in this equation will increase as the pump power and/or current density is increased essentially tracking each other. For clarity of presentation, the He_2^+ density can, therefore, be replaced by a constant times the electron density giving

$$N_2^+(B) = \frac{A n_e (N_2 k_7 + N_2 He k_8)}{n_e (k_{11} + k_{16}) + N_2 He k_{12}} \tag{6}$$

where $He_2^+ = A n_e$. Under the conditions of constant pressure and mix, as the pumping intensity and/or electron density is increased, the $N_2^+(B)$ population is found to saturate when

$$n_e (k_{11} + k_{16}) \gg N_2 He k_{12} \tag{7}$$

at a value of

$$N_2^+(B) \approx \frac{A (N_2 k_7 + N_2 He k_8)}{(k_{11} + k_{16})} \tag{8}$$

Thus, as the pumping intensity is increased by raising the charge voltage, the achievable gain is predicted to saturate. Using the rate values given in Table 1 and standard condition densities, this effect is estimated to occur at electron densities above approximately 2×10^{15} cm^{-3}, which is clearly on the same order of magnitude of concern to this study.

In Fig. 20 is shown the measured and calculated peak $N_2^+(B)$ populations as the applied voltage is raised from 55 kV to 80 kV. Saturation of the achievable upper level population is evident in both cases in which the calculated and measured populations increase by only 30 percent and 60 percent, respectively, while the energy deposition is more than doubled.[4] While by no means conclusive, these results imply that the saturation of the $N_2^+(B)$ population due to electron quenching is occurring in the present study. If this is indeed the case, it would be more desirable to discharge pump the He-N_2 system with a lower value longer duration current pulse so that gain may be sustained for a longer time, thus allowing the cavity fields time to build up to saturation. In addition, equation (8) indicates the saturated value of $N_2^+(B)$ population and therefore the maximum gain can be increased by operating at higher He pressures, thus providing another motivation for high pressure operation.

E. Comparison of Calculated and Measured Densities

With the understanding that the measured electron density is a lower limit, the peak value of the measured and predicted electron density are in reasonable agreement, as shown in Figs. 6 and 14, respectively. They clearly differ, however, in their decay rates as expected due to the constant collision frequency assumption of the absorption measurement. Assuming the electron temperature decays to 0.2 eV in the afterglow, the tail of the electron density inferred by absorption could increase by as much as a factor of four resulting in improved agreement between the calculated and measured results.

---

[4] In the case of the calculated results, the peak value of the $N_2^+(B)$ population was controlled by the saturation effect stated above while the effect of He_2^+ recombination indicated previously was evident in the temporal decay of the $N_2^+(B)$ population.
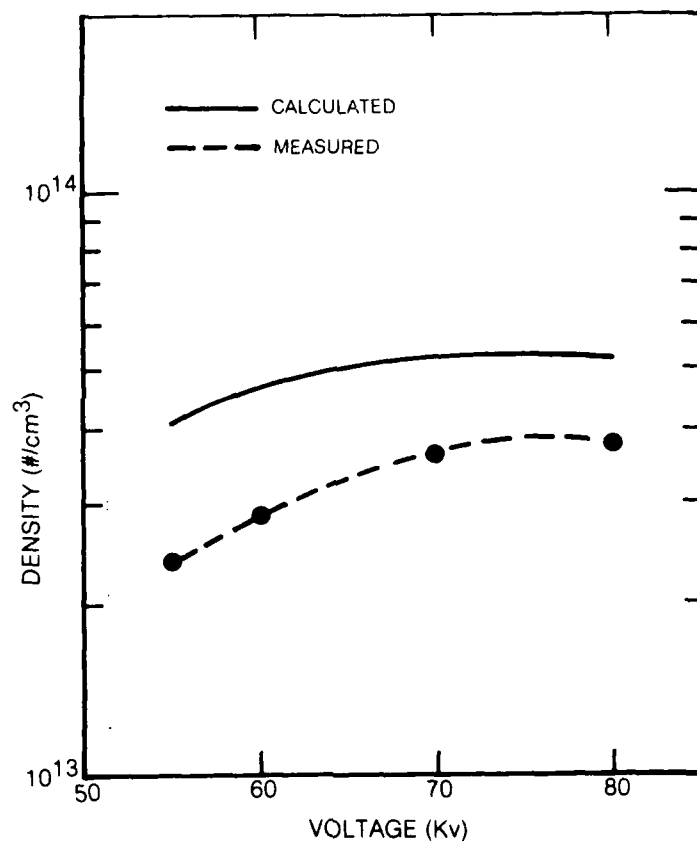
Fig. 20   Calculated and measured peak $N_2^+(B)$ population as a function of charge voltage showing saturation in the achievable population with increasing voltage.

The peak value of the measured $N_2^+(B)v = 0$ population and the predicted $N_2^+(B)$ total

population is within the experimental error of the measurement. This is not to suggest,

however, the quenching constants upon which the value of the $N_2^+(B)$ population so

critically depends are accurate; but it does suggest they are reasonable. If for

example, superelastic quenching of the $N_2^+(B)$ state were eliminated, the predicted

magnitude of the $N_2^+(X)$ and $N_2^+(B)$ state would essentially switch positions in Fig. 14.

Experimental results indicate this is clearly not the case. It is also to be noted

the predicted magnitude of the $N_2(X)$ state lies considerably above the measured

value of the $N_2(X)v = 0$ plus $N_2(X)v = 1$ population during the current pulse.

It is to be understood, however, that this is a lumped state analysis which does not

account for the vibrational distribution of states within a given electronic state.

It is, therefore, possible that a considerable fraction of the $N_2(X)$ population is hung

up in vibrational levels above the $v'' = 1$ state during the current pulse resulting in

a larger population than the experimental $v'' = 0$ and $v'' = 1$ populations indicate.

Indeed, this must be the case if an inversion on the $v' = 0 \rightarrow v'' = 0$ transition is

to occur given the predicted total populations of the $N_2^+(B)$ and $N_2^+(X)$ states.

VI. DISCUSSION AND SUMMARY

Based on the experimental and computer modeling results presented in this paper,

a general picture of the operation of the He-N_2 system excited in the capacitively

coupled capillary discharge configuration has emerged. Clearly, He$^+$ production results

mainly from a multistep ionization process with a production efficiency on the order of

15 percent. This manner of He$^+$ production results in a volumetric unstable discharge

thereby limiting the excitation pulse duration. $N_2^+(B)$ production proceeds mainly by

charge transfer from He$_2^+$ which in turn is produced by ion conversion of He$^+$. Branching

from this flow path due to He^+ charge transfer and He_2^+ recombination limited the calculated production efficiency of $N_2^+(B)$ under the present conditions to 7 percent. This upper level formation efficiency in conjunction with a 100 percent optical extraction efficiency yields a predicted laser output of 200 μJ which is considerably above the experimental estimated potential of 12 μJ-24μJ for this device. Experimental evidence was presented which indicated this discrepancy could be due to a considerable amount of lower level pumping followed by slow vibrational relaxation rather than a less than expected upper level formation efficiency. The modeling indicated lower level pumping can occur through a number of processes such as N_2 ionization, N_2^* ionization, Penning ionization, superelastic electron quenching, and charge transfer. Some of these processes are unique to discharge pumping and therefore represent a point of departure in the comparison of discharge and ,--beam pumping. Indications of slow vibrational relaxation was quite unexpected and may be a result of the capture-autoionization process proceeding at a rate in the $N_2^+(X)$ state considerable below the rate estimated for He_2^+ vibrational relaxation [11].

The model also revealed the detrimental effects of electron quenching of both He_2^+ and $N_2^+(B)$ which is generally applicable to both discharge and e-beam excitation. Under the conditions of short pulse high current excitation, He_2^+ recombination in the afterglow seriously limited the achievable $N_2^+(B)$ production efficiency through charge transfer. Superelastic quenching and recombination of the $N_2^+(B)$ state limited the achievable gain and gain duration as the applied voltage and/or energy input was increased. Likewise, observed laser output was found to be strongly limited by the magnitude and duration of the gain pulse under self-oscillating conditions due to the finite build-up time of the laser field. Indeed, optimum laser output was experimentally

found to occur for an applied voltage which resulted in a lower amplitude, longer duration current pulse and correspondingly a longer duration gain pulse. Therefore, the observed decrease in laser output with increasing charge voltage noted previously is suspected to be a result of saturation in the peak gain along with a reduction in the gain width caused by an increase in electron quenching of the He_2^+ and $N_2^+(B)$ states.

During the course of this study, a number of inconsistencies arose when the experimental results of the present investigation were compared to the previous transverse discharge results [9]. In particular, it was difficult to understand how the measured gains and saturation intensities of the two devices under identical operating conditions could be within a factor of two of each other while the pump power density of the capillary discharge was estimated to be an order of magnitude larger and laser efficiency an order of magnitude lower than inferred for transverse discharge pumping. Based on these findings, the experimental results of Collins, Carroll, and Taylor were carefully reevaluated using the present kinetic model and the equilvalent circuit [32] (see Fig. 21) of their transverse discharge device described thoroughly in Ref. [9]. Figure 22 shows a comparison of measured and calculated V-I characteristics. The energy deposition, upon which the intrinsic laser efficiency was based, was determined experimentally by integrating over the product of the V-I characteristics which corresponded to 200 mJ representing only 3 percent of the initially stored energy. On the other hand, the computed V-I characteristics predict a much larger energy deposition of 2.8 J representing 40 percent of the initially stored energy. Some of this discrepancy undoubtedly results from an over prediction of the calculated V-I characteristics. However, it was found the major portion of this discrepancy could be accounted for by a shift of only 5 nsec of the measured current curve to

52
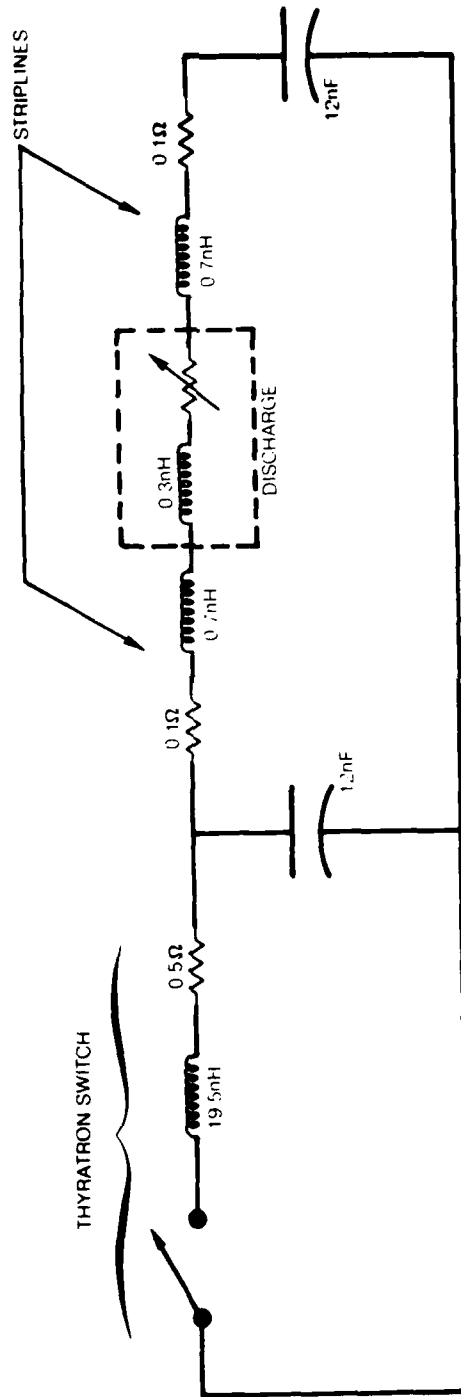
Fig. 21 Equivalent circuit for the transverse discharge pumped laser described in Ref. 9. Both electrodes of the discharge heat (dashed box) are connected to circuit board type striplines represented by the indicated series inductance, dynamic series resistance and parallel capacitance. The discharge is initiated by switching one leg of the charged striplines to ground through a thyratron which acts as an LRC circuit tending to invert the initial voltage.

80-04-120-21
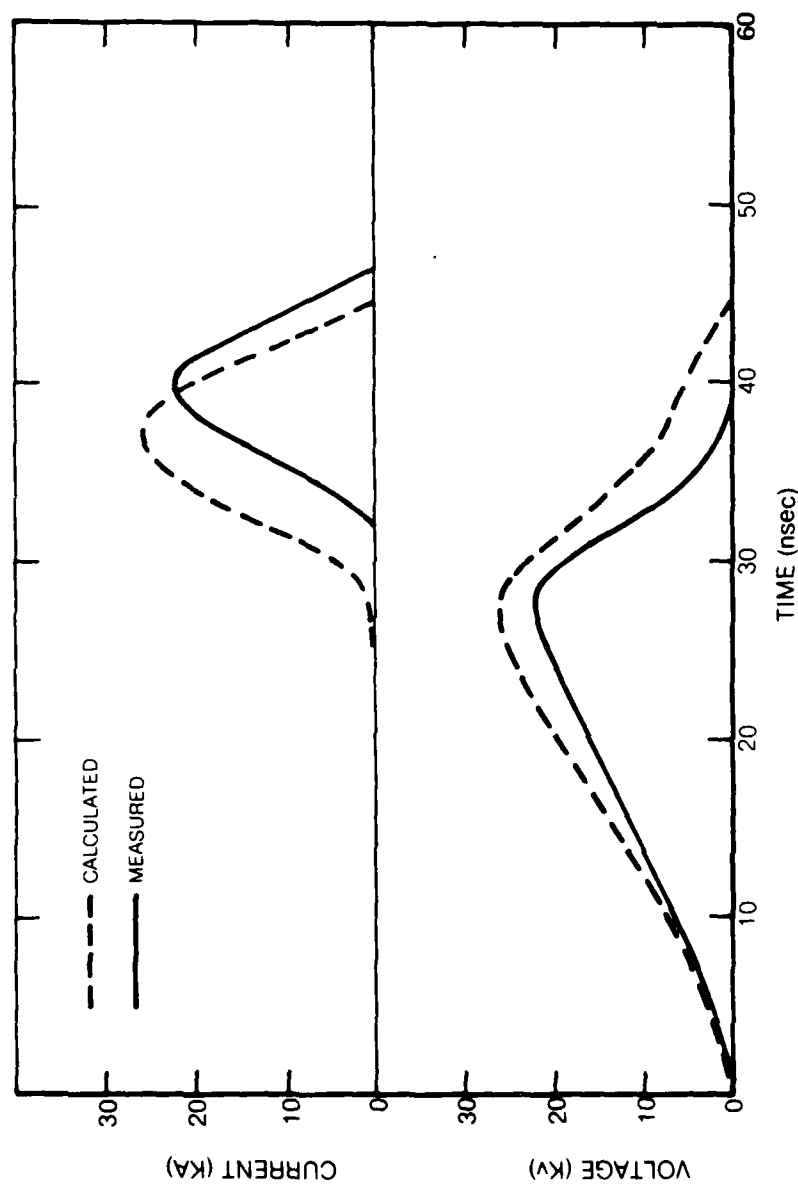
Fig. 22 Calculated and measured V-I characteristics for the transverse discharge pumped laser showing relative displacement in the timing of calculated and measured current. These results were obtained for a total pressure, charge voltage, electrode separation, and discharge area of 3.7 atms (0.15% N_2 balance He), 24 kV, 1.30 cm, and 23 cm^2, respectively.

earlier time. A shift of this magnitude would increase the energy deposition inferred by measurement to approximately 1.4 J corresponding to 20 percent of the initially stored energy. In Fig. 23 are the corresponding calculated excited state densities which can be compared to the calculated densities for the capillary discharge given in Fig. 14. This comparison reveals the general magnitude of the excited state densities of two devices to be very similar suggesting the operation of the two devices to be essentially the same. Indeed, if the capillary discharge is simply scaled to the same active volume of the transverse discharge, very similar laser output characteristics are predicted, thus implying that the estimate of a 1 percent intrinsic efficiency for the discharge pumped excited N_2^+ laser is a result of an underestimate of energy deposition.

Based on the present study as a whole, it is concluded that the discharge pumped N_2^+ laser operating in the pressure regime of this study (2 atm - 5 atm) region will be limited to device efficiencies of approximately 0.1 percent - 0.2 percent due mainly to intrinsic limitations of the $He-N_2$ system. Indeed, even the e-beam pumped N_2^+ laser was found to be inefficient in this pressure region [3],[4]. However, the modeling indicated that a number of the limitations of the $He-N_2$ system in this pressure regime could possible be overcome by operating at higher pressure due to: 1) better branching of He^+ into $N_2^+(B)$, 2) higher values of achievable gain before saturating for a given pump power density, and 3) potentially faster vibrational relaxation of the lower level. It is not unreasonable to suspect that the e-beam pumped N_2^+ laser optimized at high pressure because of these effects. It is to be understood, however, that discharge pumping at higher pressure must be accompanied by an increase in the applied voltage to hold the applied E/N at a value consistent with efficient He^* production. This may
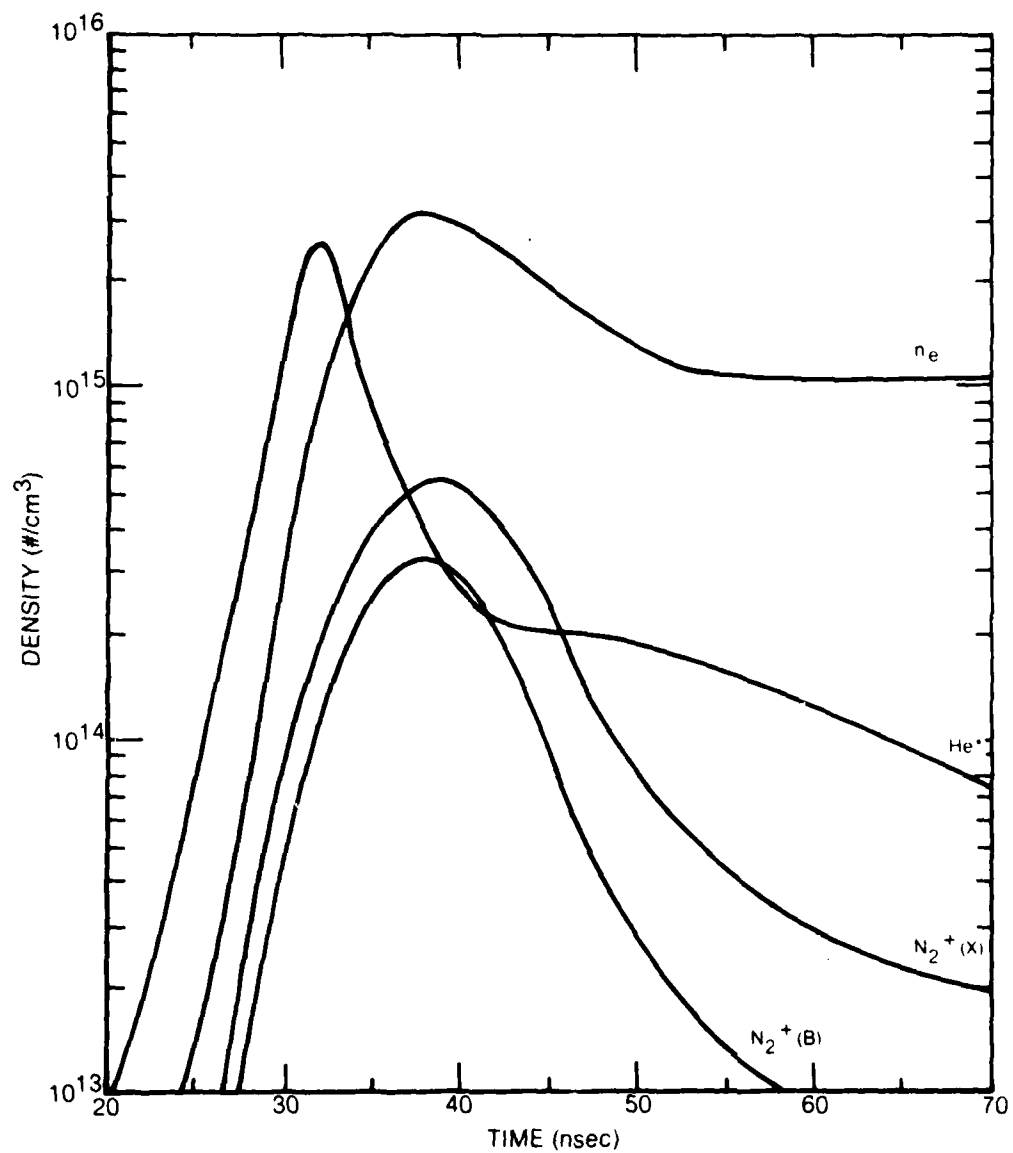
Fig. 23   Calculated densities for the transverse discharge pumped laser of Ref. 9.

require very large and therefore, impractical voltages depending upon the specific discharge geometry and application.

REFERENCES

[1]   C. B. Collins, A. J. Cunningham, S. M. Curry, B. W. Johnson, and M. Stockton, "Stimulated emission from charge-transfer reactions in the afterglow of an e-beam discharge into high-pressure helium-nitrogen mixtures", Appl. Phys. Lett., Vol. 24, pp. 477-478, 1974.

[2]   C. B. Collins, A. J. Cunningham, and M. Stockton, "A nitrogen ion laser pumped by charge transfer", Appl. Phys. Lett., Vol. 25, pp. 344-345, 1974.

[3]   C. B. Collins, "The nitrogen ion laser", Technical Reports No. UTDP ML-04 (1975); UTDP ML-05 (1976); and UTDP ML-06 (1977). Contract No. N00014-76-C-0174, The University of Texas at Dallas (unpublished).

[4]   C. B. Collins and A. J. Cunningham, "Scaling of the helium-nitrogen charge-transfer laser", Appl. Phys. Lett., Vol. 27, pp. 127-128, 1975.

[5]   C. B. Collins, J. M. Carroll, F. W. Lee and A. J. Cunningham, "Thermal modification of the kinetic sequence pumping the helium-nitrogen charge-transfer laser", Appl. Phys. Lett., Vol. 28, pp. 535-537, 1976.

[6]   V. N. Ishchenk, V. N. Lisitsin, A. M. Razhev, V. N. Starinsky, "Superradiance on the 2^+ and 1^- bands of nitrogen in a discharge at pressures above 10 atm", JETP Lett., Vol. 19, pp. 233-234, 1974.

[7]   J. B. Laudenslager, T. J. Pacala, and C. Wittig, "Electric-discharge-pumped nitrogen ion laser", Appl. Phys. Lett., Vol. 29, pp. 580-582, 1976.

[8]   D. E. Rothe and K. O. Tan, "High-power N_2^+ laser pumped by charge transfer in a high-pressure pulse glow discharge", Appl. Phys. Lett., Vol. 30, pp. 152-154, 1977.

[9]   C. B. Collins, J. M. Carroll, and K. N. Taylor, "Charge transfer pumping of the helium-nitrogen laser at atmospheric pressures in an electrical avalanche discharge", J. Appl. Phys., Vol. 49, pp. 5093-5097, 1978.

REFERENCES (Cont'd)

[10] C. H. Chen, J. P. Judish, and M. G. Payne, "Charge transfer and penning ionization of N_2, CO, CO_2 and H_2S in proton excited helium mixtures", J. Chem. Phys., Vol. 67, pp. 3376-3381, 1977.

[11] J. Stevefelt, "Three-body capture-autoionization: a mechanism for vibrational deexcitation of molecular ions in a plasma", Phys. Rev. A, Vol. 8, pp. 2507-2513, 1973.

[12] L. A. Newman, "XeF* and KrF* waveguide lasers excited by a capacitively coupled discharge", Appl. Phys. Lett., Vol. 33, pp. 501-503, 1978.

[13] R. L. Abrams, "Coupling losses in hollow waveguide laser resonators", IEEE J. Quan. Elec., Vol. QE-8, pp. 838-843, 1972.

[14] C. B. Collins, J. M. Carroll, and K. N. Taylor, "Gain and saturation of the nitrogen ion laser", Proceedings of the International Conference on Lasers, pp. 363-369, 11-15 December 1978.

[15] D. E. Shemansky and A. L. Broadfoot, "Excitation of N_2 and N_2^+ system by electrons - I absolute transition probabilities", J. Quant. Spectrosc. Radiat. Transfer, Vol. 11, pp. 1385-1400, 1971.

[16] A. Lofthus and P. H. Krupenie, "The spectrum of molecular nitrogen", J. Phys. Chem. Ref. Data, Vol. 6, pp. 113-307, 1977.

[17] J. V. Peterson, "Theoretical modeling of charge transfer lasers", Ph.D. Thesis, The University of Texas at Dallas, 1978 (unpublished).

[18] For details of this procedure, see E. J. Schimitscket and J. E. Celto, "Oscillator and oscillator-amplifier experiments with an $HgBr_2$/HeBr dissociation laser", Appl. Phys. Lett., Vol. 36, pp. 176-178, 1980.

REFERENCES (Cont'd)

[19] L. A. Newman, M. R. Schubert, and T. A. DeTemple, "FIR absorption determination of transient electron densities in high-pressure ionizer-sustainer lasers", J. Appl. Phys., Vol. 47, pp. 4904-4910, 1976.

[20] S. A. Lawton, J. B. Richards, L. A. Newman, L. A. Specht, and T. A. DeTemple, "The high-pressure neutral infrared xenon laser", J. Appl. Phys., Vol. 50, pp. 3888-3897, 1979.

[21] T. H. Johnson, L. J. Palumbo, and A. M. Hunter, "Kinetics simulation of high-power gas lasers", IEEE J. Quan. Elec., Vol. QE-15, pp. 289-301, 1979.

[22] A. E. Greene and C. A. Brau, "Theoretical studies of UV-preionized transverse discharge KrF and ArF lasers", IEEE J. Quan. Elec., Vol. QE-14, pp. 951-957, 1978.

[23] L. A. Newman and T. A. DeTemple, "Electron transport parameters and excitation rates in N_2", J. Appl. Phys., Vol. 47, pp. 1912-1915, 1976.

[24] D. C. Cartwright, S. Trajmar, A. Chutjian and W. Williams, "Electron impact excitation of the electronic states of N_2. II. Integral cross sections at incident energies from 10 to 50 eV", Phys. Rev. A., Vol. 16, pp. 1041-1051, 1977.

[25] L. J. Kieffer, "A compilation of electron collision cross section data for modeling gas discharge lasers", JILA Information Center Report 13, University of Colorada, Boulder, CO., 1973.

[26] D. Ton-That and M. R. Flannergy, "Cross sections for ionization of metastable rare-gas atoms (Ne*, Ar*, Kr*, Xe*) and of metastable N_2*, CO* molecules by electron impact", Phys. Rev. A, Vol. 15, pp. 517-526, 1977.

[27] D. R. Long and R. Geballe, "Electron-impact ionization of He ($2s$ ^3S)", Phys. Rev. A, Vol. 1, pp. 260-265, 1970.

REFERENCES (Cont'd)

[28]   V. G. Anicich, "Product distributions for some thermal energy charge transfer reactions of rare gas ions", J. Chem. Phys., Vol. 67, pp. 4340-4350, 1977.

[29]   H. H. Michels (private comminucations).

[30]   R. Deloche, P. Monchicourt, M. Cheret, and F. Lambert, "High-pressure helium afterglow at room temperature", Phys. Rev. A, Vol. 13, pp. 1140-1176.

[31]   M. Gand, A. Bouchoule, and J. Stevefelt, "Kinetics of vacuum-ultraviolet continuum from a high-pressure He fast discharge", Appl. Phys. Lett., Vol. 35, pp. 50-52, 1979

[32]   C. B. Collins (private communications).

[33]   F. W. Lee and C. B. Collins, "Measurement of the rate coefficients for the bimolecular and thermolecular deexcitation reactions of $He(2^3S)$ with Ne, Ar, N_2, CO, CO_2 and CH_4", J. Chem. Phys., Vol. 65, pp. 5189-6115, 1976.

[34]   W. C. Richardson and D. W. Setser, "Penning ionization optical spectroscopy: metastable helium (He 2^3S) atoms with nitrogen, carbon monoxide, oxygen, hydrogen chloride, hydrogen bromide, and chlorine", J. Chem. Phys., Vol. 58, pp. 1809-1825, 1973.

[35]   F. W. Lee, C. B. Collins, and R. A. Waller, "Measurement of the rate coefficients for the bimolecular and thermolecular charge transfer reactions of He_2^+ with Ne, Ar, N_2, OC, CO_2 and CH_4", J. Chem. Phys., Vol. 65, pp. 1605-1615, 1976.

[36]   A. Good, "Third-order ion-molecule clustering reaction", Chemical Reviews, Vol. 75, pp. 561-583, 1975.

[37]   J. N. Bardsley and M. A. Biondi, "Dissociative recombination", in Advances in Atomic and Molecular Physics, (Academic Press, NY), Vol. 6, pp. 1-57, 1970.

[38]   D. H. Douglas-Hamilton, "Recombination rate measurements in nitrogen", J. Chem. Phys., Vol. 58, pp. 4820-4823, 1973.

ACKNOWLEDGEMENT

REPORTS DISTRIBUTION LIST FOR ONR PHYSICS PROGRAM OFFICE
UNCLASSIFIED CONTRACTS

Director   3 copies
Defense Advanced Research Projects Agency
Attn: Technical Library
1400 Wilson Blvd.
Arlington, Virginia 22209

Office of Naval Research   3 copies
Physics Program Office (Code 421)
800 North Quincy Street
Arlington, Virginia 22217

Office of Naval Research   1 copy
Assistant Chief for Technology (Code 200)
800 North Quincy Street
Arlington, Virginia 22217

Naval Research Laboratory   3 copies
Department of the Navy
Attn: Technical Library
Washington, D. C. 20375

Office of the Director of Defense   3 copies
   Research and Engineering
Information Office Library Branch
The Pentagon
Washington, D. C. 20301

U. S. Army Research Office   2 copies
Box 12211
Research Triangle Park
North Carolina 27709

Defense Documentation Center   12 copies
Cameron Station (TC)
Alexandria, Virginia 22314

Director, National Bureau of Standards   1 copy
Attn: Technical Library
Washington, DC 20234

Commanding Officer   3 copies
Office of Naval Research Branch Office
536 South Clark Street
Chicago, Illinois 60605

Commanding Officer   3 copies
Office of Naval Research Branch Office
1030 East Green Street
Pasadena, California 91101

San Francisco Area Office   3 copies
Office of Naval Research
One Hallidie Plaza
Suite 601
San Francisco, California 94102

Commanding Officer   3 copies
Office of Naval Research Branch Office
666 Summer Street
Boston, Massachusetts 02210

New York Area Office   1 copy
Office of Naval Research
715 Broadway, 5th Floor
New York, New York 10003

Director   1 copy
U. S. Army Engineering Research
  and Development Laboratories
Attn: Technical Documents Center
Fort Belvoir, Virginia 22060

ODDR&E Advisory Group on Electron Devices   3 copies
201 Varick Street
New York, New York 10014

Air Force Office of Scientific Research   1 copy
Department of the Air Force
Bolling AFB, D. C. 22209

Air Force Weapons Laboratory   1 copy
Technical Library
Kirtland Air Force Base
Albuquerque, New Mexico 87117

Air Force Avionics Laboratory   1 copy
Air Force Systems Command
Technical Library
Wright-Patterson Air Force Base
Dayton, Ohio 45433

Lawrence Livermore Laboratory   1 copy
Attn: Dr. W. F. Krupke
University of California
P. O. Box 808
Livermore, California 94550

2

Harry Diamond Laboratories   1 copy
Technical Library
2800 Powder Mill Road
Adelphi, Maryland 20783

Naval Air Development Center   1 copy
Attn: Technical Library
Johnsville
Warminster, Pennsylvania 18974

Naval Weapons Center   1 copy
Technical Library (Code 753)
China Lake, California 93555

Naval Training Equipment Center   1 copy
Technical Library
Orlando, Florida 32813

Naval Underwater Systems Center   1 copy
Technical Library
New London, Connecticut 06320

Commandant of the Marine Corps   1 copy
Scientific Advisor (Code RD-1)
Washington, DC 20380

Naval Ordnance Station   1 copy
Technical Library
Indian Head, Maryland 20640

Naval Postgraduate School   1 copy
Technical Library (Code 0212)
Monterey, California 93940

Naval Missile Center   1 copy
Technical Library (Code 5632.2)
Point Mugu, California 93010

Naval Ordnance Station   1 copy
Technical Library
Louisville, Kentucky 40214

Commanding Officer   1 copy
Naval Ocean Research & Development Activity
Technical Library
NSTL Station, Mississippi 39529

Naval Explosive Ordnance Disposal Facility   1 copy
Technical Library
Indian Head, Maryland 20640

Naval Ocean Systems Center   1 copy
Technical Library
San Diego, California 92152

Naval Surface Weapons Center   1 copy
Technical Library
Dahlgren, Virginia 22448

Naval Surface Weapons Center (White Oak)   1 copy
Technical Library
Silver Spring, Maryland 20910

Naval Ship Research and Development Center   1 copy
Central Library (Code L42 and L43)
Bethesda, Maryland 20084

Naval Avionics Facility   1 copy
Technical Library
Indianapolis, Indiana 46218

Director, Physics Program   1 copy
Physical Sciences Division
Office of Naval Research
800 North Quincy Street
Arlington, Virginia 22217
ATTN: M. B. White
Ref: Contract N00014-79-C-0309

Air Force Plant Representative Office   1 copy
(OL-AA), Pratt & Whitney Aircraft Group
East Hartford, CT 06108

Director, Naval Research Laboratory   6 copies
ATTN: Code 2627
Washington, D. C. 20375

Office of Naval Research Branch Office   1 copy
666 Summer Street
Boston, Massachusetts 02210